Understanding the electrode-electrolyte interfaces of ionic liquids and deep eutectic solvents

Oguz Kagan Coskun, Miguel Munoz, Saudagar Dongare, William Dean†, Burcu E. Gurkan*

*** E-mail: beg23@case.edu**

Chemical and Biomolecular Engineering, Case Western Reserve University, Cleveland, Ohio, USA

ABSTRACT: Developing unconventional electrolytes such as ionic liquids (ILs) and deep eutectic solvents (DESs) has led to remarkable advances in electrochemical energy storage and conversion devices. However, the understanding of the electrode-electrolyte interfaces of these electrolytes, specifically the liquid structure and the charge/electron transfer mechanism and rates, is lacking due to the complexity of molecular interactions, the difficulty in studying the buried interfaces with nanometer-scale resolution, and the distribution of the timescales for the various interfacial events. This Feature Article outlines the standing questions in the field, summarizes some of the exciting approaches and results, and discusses our contributions to probing the electrified interfaces by electrochemical impedance spectroscopy (EIS), surface-enhanced Raman spectroscopy (SERS), and neutron reflectivity (NR). The related findings are analyzed within electrical double-layer models to provide a framework for studying ILs, DESs, and, more broadly, the concentrated hydrogen-bonded electrolytes.

INTRODUCTION

Interfaces form ubiquitously in nature when a solution interacts with a metal, semiconductor, polymer or another solution, resulting in a double-layer of balanced opposing charges on both sides.[1] Electrochemists are motivated to characterize these interfaces to understand the excess charge accumulation as it relates to electron transfer reactions in electrocatalysis, electrodeposition, energy storage and conversion processes, among others. To develop a physical model of the interface, configurations of the ions, dipoles, and neutral molecules, as well as the variation of actual and perturbed species concentrations with distance from the electrode, are needed.[2]

The electrical double-layer (EDL) models aim to combine the solid-state theory of the electrode to capture the nature of electrons and the statistical mechanics of the electrolyte to describe the interface.[3] The traditional view of a dilute electrolyte is that many water or solvent molecules form solvation sheaths around the dissociated ions[4] with negligible ion-ion interactions. Classical double-layer theories such as Helmholtz[5] and Gouy-Chapman[6]-Stern[7] sufficiently describe the interface for dilute electrolytes. Concentrated electrolyte classes, such as ionic liquids (ILs) and deep eutectic solvents (DESs), challenge this traditional view of an electrolyte since there are significant ionic interactions[8-10] in addition to surface-specific interactions and voltage-induced ion orientations at the electrode-electrolyte interface.[11, 12]

ILs are distinguished from molten salts by the criteria of melting below 100 °C.[13] ILs have a wide liquidus range, low or negligible volatility, tunable solvation strength, and wide electrochemical stability window that enable access to electrochemical processes that cannot be achieved with aqueous or non-aqueous organic electrolytes. DESs exhibit properties similar to ILs and form upon mixing of Lewis or Brønsted acids and bases; often these constituents can be hydrogen bond acceptors (HBAs) and hydrogen bond donors (HBDs) at a specific composition that results in a liquid with a significantly depressed freezing point.[14] Common HBDs are alcohols, amines, and amides, and common HBAs are halide salts.[15] Though there is some uncertainty about the exact composition of these mixtures to fulfill the definition of a DES,[16] these concentrated electrolytes are of interest for many applications due to their tunable properties and low volatility owing to their hydrogen bonding network. Structures of the ILs and DESs mentioned in this article are given in **Figure 1**.

A few example applications of ILs and DESs involving an interface include metal deposition, batteries, extractions/separations and electrocatalysis.[17] In these applications, performance metrics such as current density, Faradaic efficiency, and deposit morphology are impacted by the interfacial structure, which determines the charge distribution and influences the likeliness and the rate of an interfacial reaction. Therefore, to understand electro-kinetics in ILs and DESs, a sufficient description of the interface including surface adsorbed species and charge distribution is needed. An excellent review of the EDL theories and their applicability to ILs was written by Fedorov and Kornsyshev in 2014.[18] Later in 2020, Kornsyshev, Bazant, and co-workers[19] presented an EDL model to couple the steric and electrostatic forces in ILs that predicted discrete ion layers with decaying oscillations along the perpendicular direction away from the polarized electrode. Nonetheless, extended studies and theoretical frameworks are lacking for interfaces with concentrated hydrogen-bonded electrolytes such as DESs. There are several unanswered or debated questions in the field: (1) How to describe the IL/DES-electrode interfaces as a function of molecular functionality and composition?; (2) What is the interfacial thickness and how is the liquid structured?; (3) What is the role of hydrogen bonding on potential-dependent capacitance?; (4) What are the surface species (e.g., specifically adsorbed on the electrode) and how do they impact electron transfer?; (5) Can a new EDL model be developed to effectively capture DES behavior under polarization?; (6) What is the origin of hysteresis in EDL formation with changing potential sweep direction?

Transient voltammetry techniques such as cyclic voltammetry (CV) and electrochemical impedance spectroscopy (EIS) offer a means to investigate the interfacial phenomena, including charge transfer kinetics[20] and potential-dependent capacitive behavior[21]. However, studying these phenomena in concentrated and highly viscous electrolytes such as ILs and DESs presents challenges compared to aqueous

systems. Factors such as reference electrode stability and compatibility,[22] ohmic drop, and mass transfer limitations must be carefully considered.[20, 23] Therefore, new approaches beyond the classical electrochemical methods are needed to answer the questions posed above and there is a need to integrate advanced characterization techniques (e.g., spectroscopy) with appropriate electrochemical methods.

Recently, a wider range of techniques has been used to study ILs at interfaces. Scanning tunneling microscopy (STM) has been used to investigate the lateral arrangement of ions in the interface with limited success due to insufficient atomic resolution.[24, 25] Fourier Transform Infrared Spectroscopy (FTIR),[26] Surface Enhanced Infrared Absorption Spectroscopy (SEIRAS),[27] Shell Isolated Nanoparticle Raman Spectroscopy (SHINERS),[28] Surface Enhanced Raman Spectroscopy (SERS),[29-31] Sum Frequency Generation (SFG),[32-34] and Neutron Reflectivity (NR)[35] have been demonstrated for probing the interface and acquiring a compositional knowledge to complement the electrochemical techniques. However, theoretical guidance in interpreting and analyzing the data from these advanced techniques is still needed in order to develop a unified understanding.

In this Feature Article, a current understanding of the interfacial structure involving ILs and DESs enabled by various approaches is introduced and the specific EDL theories developed to describe these concentrated electrolytes are briefly introduced. The significance to the electrode-electrolyte interfaces on electron/charge transfer reactions in energy storage devices and electrocatalytic reactions utilizing IL and DES electrolytes is discussed. Our contributions in probing and modeling these interfaces are highlighted.

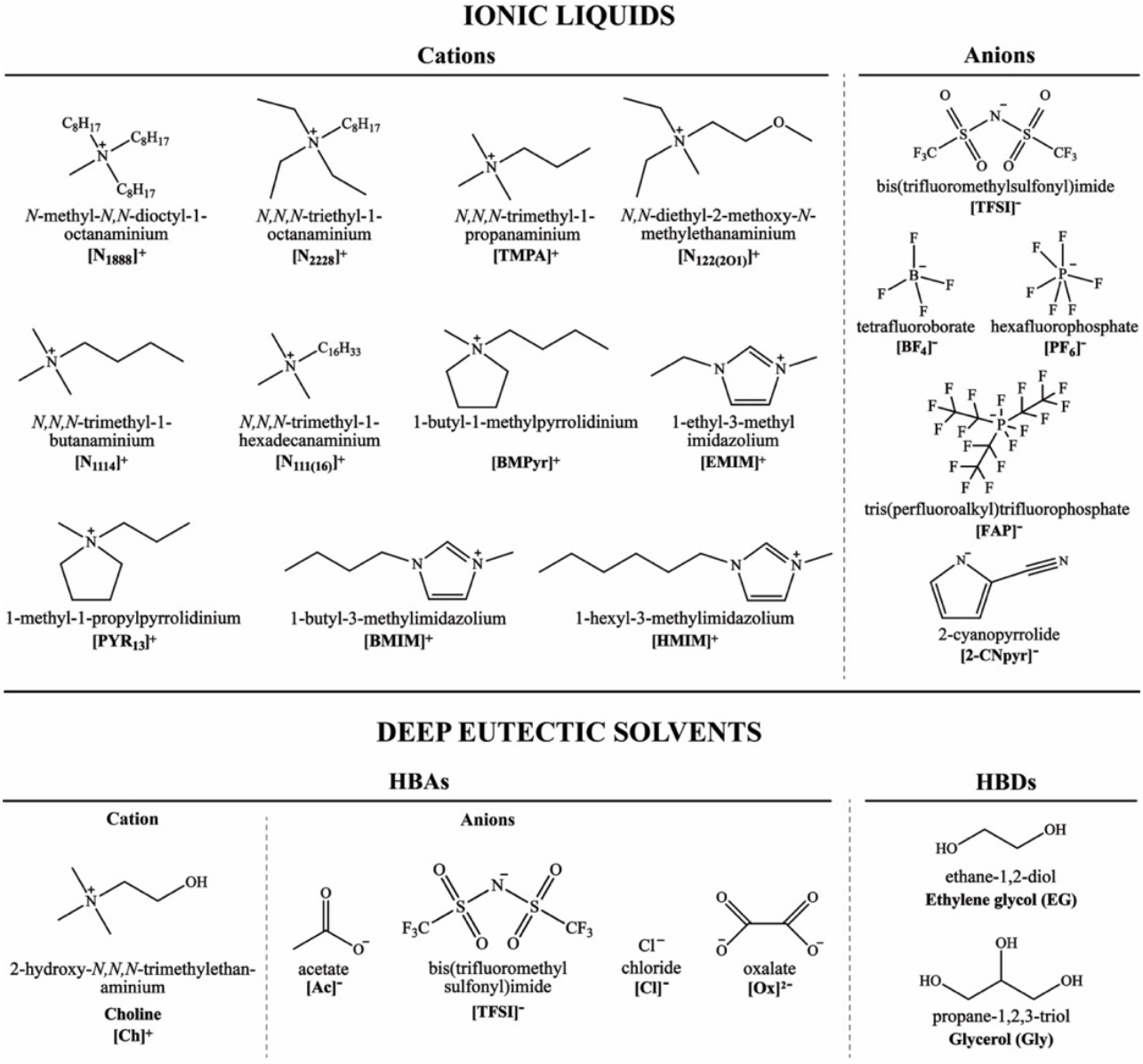

Figure 1. Molecular structure, full/abbreviated names of common anions and cations for ILs, and hydrogen bond acceptors (HBAs) and donors (HBDs).

WHAT ARE THE DIFFERENCES WITH INTERFACES FORMED WITH ILs and DESs *vs.* DILUTE ELECTROLYTES?

The formation of an electric double layer at the electrode-electrolyte interface has been studied since the early days of electrochemistry. Helmholtz introduced the first conceptual picture of this interface in 1853 as a simple capacitor formed by ions in the electrolyte side attracted by the oppositely charged surface, creating a well-defined plane-like arrangement. Gouy and Chapman re-evaluated this arrangement by considering the entropic effects, proposing a diffuse charge zone where charge density diminishes with distance from the electrode towards the bulk.[6] This model has been shown to accurately describe electrolytes with low ion concentrations at applied voltages around the point of zero charge (PZC) when there is no specific adsorption on the electrode surface. Potential-dependent capacitance curves assume a U-shape in this model. Since the model excludes the ion volume, the charge can be stored infinitely at high voltages, which is unrealistic. Stern combined these two approaches with a 'Helmholtz-like' compact layer which avoided the infinitely increasing differential capacitance curves at higher voltages.[7] Nevertheless, these earlier models fail to explain the complex interfacial behavior of ILs where camel-shape and even bell-shape capacitance curves have been reported since a combination of van der Waals, Coulomb, dipole, and solvophobic forces are at play.[36] While similar shapes in capacitance curves have been reported for aqueous systems, the underlying phenomenon differ. To understand these differences, it is best to first describe the traditional view of the EDL and the significance of PZC in dilute aqueous systems.

At PZC, the electric field near the surface nearly diminishes, except for a dipolar effect arising from the interaction between water and the electrode. Water possesses a dipole moment, and the presence of surface charge leads to a preferential orientation of water molecules near the interface, depending on the surface charge.[37] When water molecules adsorb onto an electrode surface, their orientation can significantly impact the PZC of that interface. Specifically, at low potentials below the PZC, hydrogen atoms of water tend to orient towards the surface, whereas at potentials more positive to the PZC, oxygen atoms face the surface. This reorientation of water molecules at the interface can influence the overall charge distribution, thereby causing a shift in the PZC. It is important to note that the specific adsorption of ions and the reorientation of water dipoles are interrelated phenomena that exert a critical influence on the interfacial capacitance behavior.[38] Bockris and colleagues recognized that the dipole moment of water plays a pivotal role in the EDL dynamics[39], and introduced the Bockris, Devanathan and Müller (BDM) model that accounts for a different dielectric constant in the first and second water layers at the interface.[40] So far, it is not clear how the dielectric effects influence the EDL in the case of ILs and DESs as they both present widely varied structures and compositions.

When examining scenarios involving basic and inert metals in non-specifically adsorbing dilute electrolytes, such as the case of mercury (Hg) immersed in aqueous solutions of sodium fluoride (NaF)[41] or sodium dihydrogen phosphate (NaH_2PO_4)[42], the determination of the PZC can be accomplished by analyzing experimental differential double-layer capacitance curve within the G-C framework where the minimum corresponds to PZC. With ILs and DESs, the PZC is often more challenging to determine as there may be no clear minimum in the capacitance curve. This is believed to be related to specific ion adsorption.

The pioneering work of Valette and Hamelin on Ag[43-45] and Au[46] electrodes with diverse crystallographic orientations, immersed in aqueous electrolytes like sodium perchlorate ($NaClO_4$), potassium hexafluorophosphate (KPF_6), and potassium tetrafluoroborate (KBF_4), has yielded insights into the impact of adsorbing electrolytes on EDL behavior. They reported a distinct double peak formation (*camel-shape*) around PZC of the capacitance curve. This was later explained by Shin et al.[47], through molecular dynamics (MD) simulations, as the change in charge-separation distance due to specific ion adsorption and the alteration of the orientation of the water dipoles leading to a change in the effective dielectric constant. Consequently, a maximum in capacitance was observed both in negative and positive polarizations, thus forming the peaks on both sides of the PZC minima, likened to the two-humps on camel, hence referred as the camel-shape. Further, Pajkossy et al. [48] observed only a single peak formation (*bell-shape*) with the more reactive metal Pt (111) electrode immersed in potassium perchlorate ($KClO_4$) and NaF solutions. The authors attributed the peak formation to the reorientation of the water dipole layer and the chemisorption of the water at the interface.

In concentrated electrolytes, as the ions are associated to a degree, the potential-dependent capacitance hence the shape of the curve is highly dependent on the short-range interactions. However, it has been shown that long-range electrostatic forces in ILs can also play a role at the surface. Gebbie et al.[49] reported long-range interactions at mica and gold (Au) surfaces for ILs as measured by surface force apparatus (SFA). Long-range interactions show IL-dependent exponential decay, with lengths ranging from 5 to 10 nm for many ILs.[50-53] Despite differences in short-range structuring, the similar decay lengths imply a common mechanism in the long-range force regime. Gebbie et al. also studied the temperature dependance of long-range interaction forces through SFA.[50] The near-surface bound ion layers remained unchanged with temperature, while the interaction decay length systematically decreased as the temperature was increased from 22 to 75 °C. This was explained through the disruption of ionic correlations at elevated temperatures, thus enabling ions to screen surfaces over shorter distances more readily.[50] These studies highlight that short-range structuring and long-range interactions are commonly present in ILs and the composition, surface, and external conditions highly influence the short- and long-range double layer regime. However, the earlier interpretation of the long-range electrostatics displayed by ILs exceeding the theoretical Debye length was likened to dilute electrolytes which was controversial and led to further discussions and revisit of the topic in 2017 by Rutland, Israelachvili, Perkin, Atkin, and colleagues.[54] It was discussed that the ionic associations are too strong in ILs that only a small fraction of ions acts as free charge carriers. Therefore, large decay lengths emerge as the interaction between two central ions through their surrounding counterion clouds is effectively lowered. This was referred as the charge renormalization

and linked to permittivity of the liquid following a scaling law.[55] Nevertheless, the origin of long-range forces in ILs remains debated as the charge renormalization could not explain all of the literature data and the hysteresis in capacitance curves with changing direction of the polarization.[56, 57]

Atkin and colleagues studied the interfacial structure of ILs formed on atomically flat model substrates, including graphite, mica, and silica, with atomic force spectroscopy (AFS).[58] The oscillations in the force separation curves were found to correlate with the ion dimensions. Further, the layered interfacial structure was observed to be a strong function of the surface charge and roughness. Other studies utilizing X-ray reflectometry (XR)[59] and SFA[60] also confirmed the presence of multiple alternating layers of cations and anions perpendicular to the interface between IL and electrode, where interfacial layering was found to extend from 3-4 up to 12 layers.[61, 62] This layering behavior is in contrast to dilute electrolytes where a single compact layer on the electrode surface is followed by a diffuse ion layer. The specific structural arrangement also varies depending on the substrate material. For instance, angle-resolved XPS studies have shown that on a Ni (111) surface, [MMIM][TFSA] adsorb with the cations lying flat against the surface and the anions positioned above the imidazolium rings.[63] Conversely, on an Au (111) surface, the anions are observed to be located between the cations, both in direct contact with the surface but with the anions slightly elevated above the cations. [64]

More recently, Espinoza-Marzal and colleagues[65] reported on the reorganization of ions in ILs that occur over time scales of 20 hrs and length scales of 10 nm that impacts evolution of EDL, which offers some explanation as to the origin of the reported capacitive hysteresis and the governing role of non-electrostatic interactions besides the electrostatic in ILs undergoing phase transformation. Interestingly, Blanchard and coworkers reported the presence a long-range free charge density gradient in ILs (approximately 100 μm), the magnitude and the extent of which is a rare occurrence in liquid solvents.[66] They later showed that the free charge density depends on the alkyl chain length of the cation (i.e., substitution on the imidazolium) and greater for $[TFSI]^-$ than $[BF_4]^-$ anion as examined by fluorescence anisotropy decay measurements.[67]

The interfacial ion arrangement in ILs are often described by two phenomena: overscreening and crowding.[68] When the charge on the electrode surface is infinitesimally small, the first electrolyte layer near the electrode results in a larger counter-ion charge than the one required to screen the charge on the surface. Consequently, the second layer over-compensates the excess charge accumulation in the first ion layer. This results in more charge accumulation in the second layer than the charge difference between the electrode and the first layer. These charge oscillations extend over several layers until they fade into the bulk electrolyte. This phenomenon is called overscreening. The oscillating layers of ions caused by overscreening were first reported by Mezger et al.[59] on the sapphire (0001) surface. On the other hand, when the charge on the electrode is too high, counter-ions cannot screen this charge on the electrode in a single monolayer due to geometric restrictions of the bulky cations and anions of ILs; thus, they form a multi-layer of the same counter-ion next to the electrode surface. This behavior of multi-layer of the same charge accumulation is called crowding. In computational studies[19] where a radial distribution of ions as a function of distance from the electrode surface clearly demonstrates the said layering and the overscreening vs. crowding phenomena. However, in the light of ionic interactions and real ion volumes, it is difficult, if not impossible, to observe the same in experiments.

The presence of a layered structure is also strongly influenced by the roughness of the electrode surface. This poses a challenge in experimentally observing the arrangements of ions in distinct layers, as the length scale of interfacial structures and surface roughness can be similar. Neutron reflectivity (NR) is a powerful technique that detects variations in the scattering length density (SLD) of layered materials with sub-nanometer precision. If the electrode-electrolyte interface of ILs is modeled as a layered material with varying SLD, NR can provide valuable insights to the number and thickness of each ion layer. However, liquids hardly behave as solids and the accurate detection of the compositional changes in the liquid due to ion layers require atomically smooth surfaces to prevent the propagation of surface roughness into the liquid.

In our recent study, Klein et al.,[35] we minimized the surface roughness by utilizing Si surfaces to study the interfacial behavior of $[N_{1888}][TFSI]$ by NR. Si surfaces were chemically modified to achieve a native surface charge to mimic polarization on the electrode surface. The SLD profiles and reflectivity obtained with Si substrate modified with sputter-coated Au (left) and chemically deposited Au (right) are shown in **Figure 2**. It can be seen that the Au surface obtained by sputter coating on Si, labeled as $(Au\text{-}Si)_s$, results in fringes in the reflectivity data due to the rough Au surface. This roughness is greatly diminished in the chemically deposited Au case, $(Au\text{-}Si)_{cd}$, thus allowing for improved resolution and reduced residuals between the SLD model and the reflectivity data. These results are promising in terms of probing IL-electrode interfaces by NR. However, there are still challenges as the potential-dependent restructuring may result in even smaller nuances in the reflectivity. Therefore, a synergistic approach that leverages both advanced experimental techniques and accurate modeling by molecular dynamic simulations is still necessary to develop realistic SLD models to fit the reflectivity data to extract information from subtle changes in NR and describe the interface through multiple layers instead of one diffuse layer.

In contrast to ILs, studies on DESs are scarce. A few reports found the bulk liquid structure of DESs to be more structured than ILs,[69, 70] and the interfacial studies measuring capacitance curves presented less dependence on polarization, compared to ILs. Figueiredo et al.,[71] examined glyceline DES composed of choline chloride (ChCl) and glycerol (1:2 molar ratio) on Pt, Au, and glassy carbon (GC) where very small capacitance changes were noted with varied potentials; although potential dependent curves were dramatically different between the electrodes, demonstrating a larger capacitance on Au, and Pt possibly due to specific absorption of species. Costa et al.[72] also examined similar DESs based on ChCl as the HBA on mercury electrode and suggested that the cations approach the electrode surface with

their solvation shells composed of the HBD molecules, thus forming an inner layer on the electrode composed of HBDs. To further understand the surface species, advanced spectroscopic techniques and molecular dynamics (MD) simulations were employed. Vieira et al.[73] utilized polarization modulation infrared reflection absorption spectroscopy (PM-IRRAS) to investigate the adsorption of ethaline, ChCl:EG (1:2), on a GC electrode. Their time-resolved measurements at open circuit potential indicated the self-assembly of the DES at the surface. Stepping towards negative polarizations revealed Ch^+ adsorption on the surface with a tilted orientation, while stepping towards positive polarizations led to a vertically oriented Ch^+ adsorbed layer; in addition to a strongly adsorbed EG layer. Chen et al.[74] employed AFM to study pure Gly and EG, and the corresponding DESs with ChCl, (i.e., glyceline and ethaline, respectively) on highly oriented pyrolytic graphitic electrodes. They reported again an adsorbed HBD layer on the electrode. The calculated average packing dimensions for innermost layer of pure Gly and EG were 0.5 and 0.45 nm, respectively. Meanwhile, the measured layer thicknesses were found to be 0.3 nm for Gly and 0.2 nm for EG, indicating a Gly and EG enriched inner-layer where HBDs lie flat along the surface. In a separate investigation, Wu et al. [75] explored the adsorption behavior of ethaline DES on Au(111) using shell-isolated nanoparticle-enhanced Raman spectroscopy (SHINERS) and EIS. Their findings indicated that Ch^+ and EG adsorb onto the Au surface under negative polarizations and Cl^- was observed to interact strongly with the Au electrode under positive polarizations. These observations were also corroborated by MD simulations,[76, 77] and the results suggested a specific adsorption of the neutral HBD molecules onto the electrode surfaces, leading to an inner layer of mixed HBD molecules and counter-ions, depending on the DES-electrode interactions.

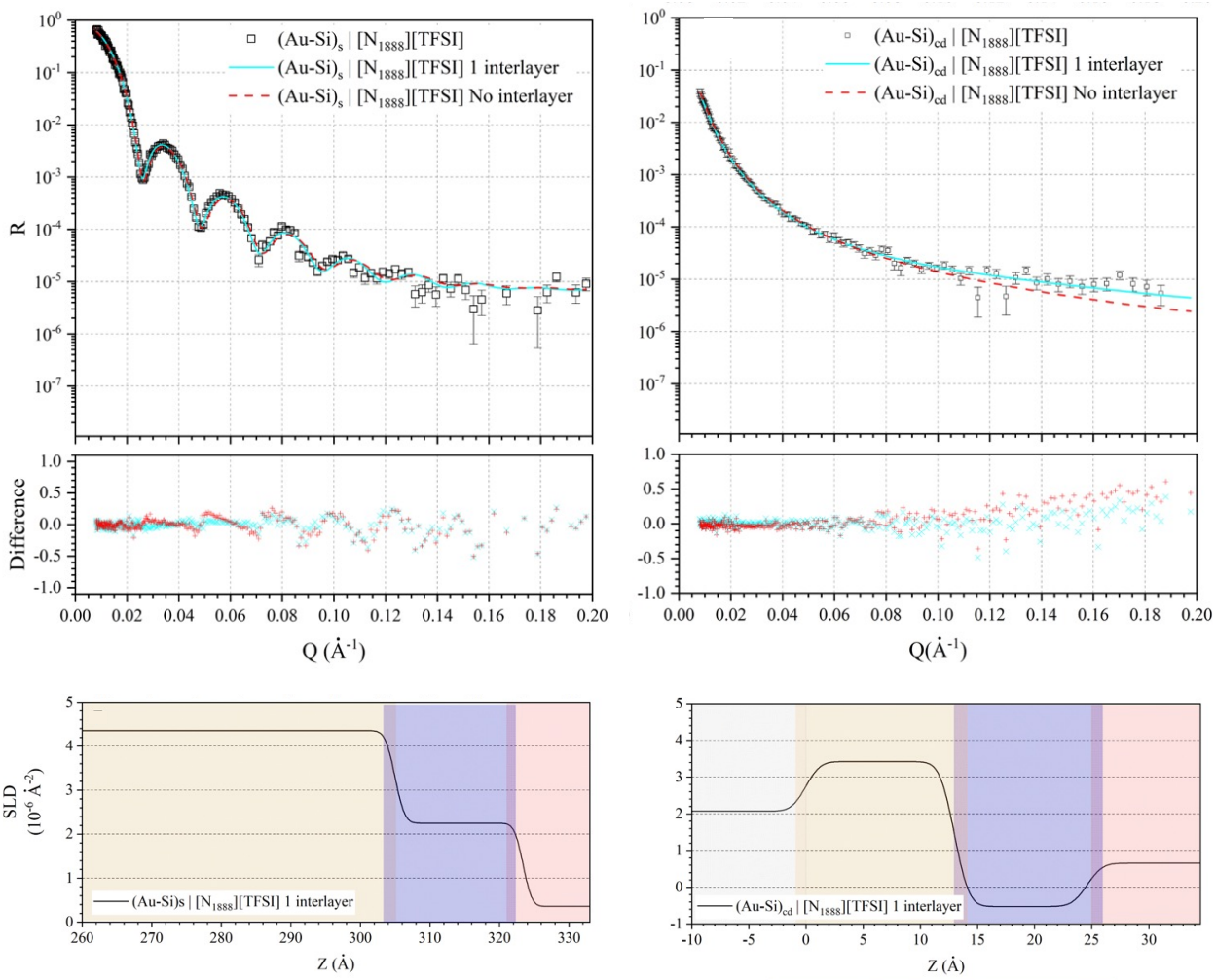

Figure 2. Reflectivity of $[N_{1888}][TFSI]$ on $(Au\text{-}Si)_s$ (left) and $(Au\text{-}Si)_{cd}$ (right). The NR data was modeled as having no electrode-electrolyte interface (bulk liquid) or 1 interfacial layer; residuals between the calculated and measured reflectivity as shown as the difference below. The bottom row with the colored-graphs show the corresponding SLD profiles with 1 interfacial layer model (purple) in between the Au electrode (gold) and bulk electrolyte (red). The overlaps between the shaded regions represent the roughness that emerge from the model. Reprinted with permission from ref. 35. Copyright 2022, American Chemical Society.

In our study with ethaline on GC, Pt, and Au electrodes, Dean et al.[21] also observed strong Cl^- adsorption on Au electrode as evident from the peak appearance on the differential capacitance curve upon positive polarization as seen in **Figure 3** while a very weak potential dependence was seen with GC and Pt electrodes. In contrast to ILs, the capacitance curves resembled more of a shallow U-shape. The theoretical framework that captures this behavior was developed by modifying the classical theories for dilute electrolytes with an additional interaction parameter that accounts for the ionic interactions as detailed in the next section.

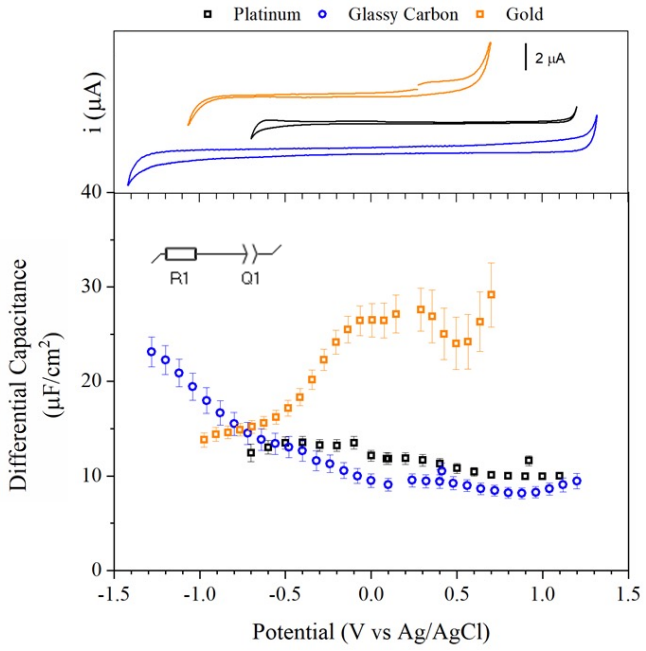

Figure 3. Differential capacitance (bottom) and CV (top) of ethaline at Pt (black), GC (blue), and Au (orange) electrodes. CV scan rate is 20 $mV.s^{-1}$. EIS was conducted over a frequency range spanning from 500 kHz to 100 mHz , utilizing an applied voltage amplitude of 20 mV. Inset schematics represent the equivalent circuit model that was fitted to the EIS data to calculate the differential capacitance. Reprinted with permission from ref. 21 under CC-BY-NC-ND license.

For ILs, the physical picture that emerges from the studies thus far is that given a negatively charged surface, the innermost layer becomes cation-rich displaying an overscreened or crowded interface, depending on the strength of ion-solid and ion-ion interactions, and the shape of the ions. The adjacent layer is then an anion-rich layer to preserve electroneutrality, which may also overscreen the preceding layer. In this way, this pattern is repeated across a few layers, resulting in ordered and alternating ion layers close to the electrode, extending a few nm away from the interface. More so for DESs, the prevailing phenomena are the specific HBD or ion adsorption to the electrode surface, lack of a clear PZC, and a weak potential-dependence in the U-shape capacitance curve on inert electrodes. **Figure 4** schematically illustrates the main differences discussed for the interfaces formed with ILs and DESs, compared to conventional dilute electrolytes. It is clear that these concentrated electrolytes cannot be evaluated with the framework of classical Gouy-Chapman-Stern theory.

INTERFACIAL MODELS

In 2007, Kornyshev[78] used the Poisson-Fermi equation to model concentrated electrolytes, particularly for describing IL interfaces. The electrolyte was treated with a mean-field lattice-gas model to analytically express the differential capacitance. Bazant and colleagues independently devised the same analytical answer by solving a modified Poisson-Nernst-Planck equation[79, 80] and proposed a comparable capacitance and potential distribution expression. Interestingly, when Oldham[81] used the same ideas as the Gouy-Chapman-Stern to model the IL-electrode interface, an identical potential profile predictions to Goodwin-Kornyshev's mean field theory was obtained for a limited number of cases.[78] Later, Bazant and Kornyshev's derived formula was modified to account for short-range forces and ion size asymmetry.[82] The resulting Goodwin-Kornyshev capacitance (C_{GK}) expression is as follows:[82]

$$C_{GK} = C_d \cosh\left(\frac{\alpha u}{2}\right) \frac{1}{1+2\gamma \sinh^2\left(\frac{\alpha u}{2}\right)} \sqrt{\frac{2\gamma \sinh^2\left(\frac{\alpha u}{2}\right)}{\ln\left(1+2\gamma \sinh^2\left(\frac{\alpha u}{2}\right)\right)}} \quad \text{eqn (1)}$$

Here, C_d is the Debye capacitance ($C_d = \alpha^{1/2}\varepsilon^*/4\pi\lambda_d$) and it is related to ε^*, the effective dielectric constant of the medium and λ_d, the Debye length. Other parameters are k_b which is the Boltzmann constant, u which is the dimensionless potential ($u = eV/k_bT$) and α which accounts for short range interactions in concentrated electrolytes such as ILs where there is no solvent ($\alpha<1$). The first part of eqn. 1 ($C_d \cosh\left(\frac{\alpha u}{2}\right)$) captures a Gouy-Chapman like behavior, leading to the formation of U-shaped capacitance curves. This part alone is sufficient for the treatment of dilute electrolytes and for small polarizations around PZC. However, to observe the behavior of ILs, which have a wider electrochemical window, the second part is needed as it captures the compacity factor, γ, and its relation with the ionic associations. Accordingly, $(1-\gamma)$ represents the proportion of free volume in ILs. This parameter has also been viewed as the fraction of mobile ions.[83, 84] When $\gamma > 1/3$, the capacitance curve represents a bell-like shape; when $\gamma < 1/3$, the curves present a double hump shape known as the 'camel' shape. This term emerges from the fact that ions are highly associated in ILs and not all ions contribute to conductivity as free ions do.

More recently, Goodwin and Korynshev[85] treated ion-pairing as a reversible process where ion pairs persist at small potentials and dissociate when the electrostatic potential is larger than the free energy of an association. The strong ionic associations leading to aggregation has also been recently treated as a percolating ionic network, hence referred as gelation. Goodwin et al.,[86] reported a similar transition from a gelled state to a regime dominated by free ions with increasing polarization of the electrode. This was likened to the transition from gelation (over screening) to crowding. Consequently, the gelled state presents a deviation from the Debye-Hückel theory; leading to longer screening lengths than those predicted by the theory. In a related context, Safran and Pincus[87] recently introduced a scaling analysis for concentrated electrolyte solutions surpassing 1 M concentration. The scaling arguments propose a linear correlation between the screening length and salt concentration, aligning with the experimental findings observed through surface force measurements.

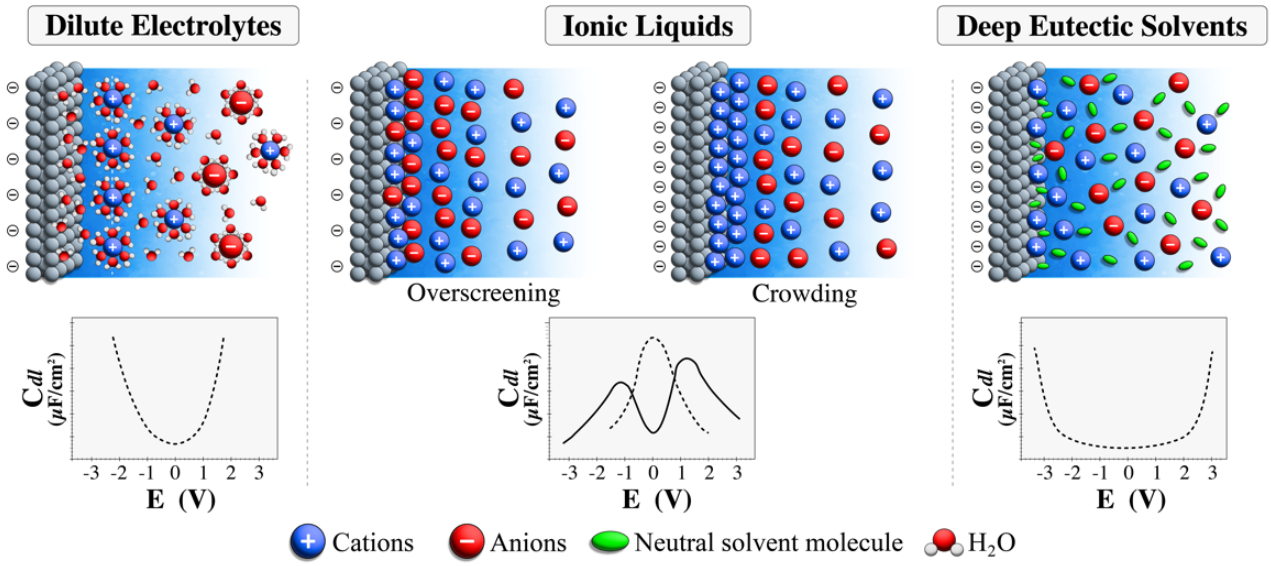

Figure 4. Schematic representations of the interface for dilute electrolytes, ILs, and DESs on a negatively charged electrode, along with their corresponding differential capacitance curves. A compact ion layer is followed by a diffuse layer for dilute aqueous electrolytes on the left. The middle panel represents the interface for ILs under overscreening and crowding. Differential capacitance curves for ILs show camel (solid line) and bell (dashed line) shapes. The right panel represents the interface for DES with specific adsorption of neutral HBD molecules on the electrode surface.

The 'bell' shape capacitance suggests the liquid has a high compacity, to begin with, and there are no voids to admit by increasing the potential, thus decreasing the capacitance immediately. In the case of 'camel' shaped capacitance curves, following an initial admission of voids and an increase in capacitance, the ability of ion packing near the electrode decreases, leading to lattice saturation (i.e., maximum capacitance). With increased polarization, ions of identical charges begin to occupy multiple layers, causing the double layer to expand and thicken, resulting in the decay of capacitance. Another aspect to consider in the theoretical framework for double layer is the varying relative permittivity. It is important to note that variations in the relative permittivity as a function of the distance from the electrode surface are well-established in dilute aqueous electrolytes; the relative permittivity of water in dilute electrolytes fluctuates from 78 in the bulk to 6 at the electrode surface.[88] Even though relative permittivity of the IL assumed to be constant regardless of the distance from the solid surface in the aforementioned GK model predicting a camel-shaped differential capacitance curve, the self-consistent mean field model developed by Lauw et al. [89] enables the polarizability of the ions comprising the IL and still predicts a camel-shaped differential. In relation to the shape of the capacitance curve, Merlet et al. [90] discussed the importance of considering not only charge density perpendicular to the interface but also the lateral distribution of charges for a comprehensive understanding of interfaces formed with concentrated electrolytes. This three-dimensional perspective of the interface was also elucidated by Kornyshev and Qiao[91], highlighting a unique feature of IL double layers where structural transitions can occur in the layer adjacent to the electrode, even without specific adsorption of its ions on the electrode surface, especially in nano-confinement.

Despite the theoretical frameworks developed to date, foreseeing the interfacial properties of an IL-electrode interface is challenging, primarily due to the difficulty in independently determining the compacity (γ) of the IL. Nevertheless, we can begin to understand the interface by probing the mobile ion layer by EIS. The strength of EIS lies in its inherent ability to probe electrochemical processes that may unfold simultaneously but across different time scales distinguishing it from DC techniques. For instance, the charging of the double-layer typically takes microseconds, while diffusion takes place on a timescale of hundreds of milliseconds.[92] However, the interpretation of the EIS data needs to be performed with care. EIS data for electrochemical systems without a Faradaic reaction is typically analyzed by an equivalent circuit model representation such as a simple R-C circuit (R stands for a resistor and C stands for a capacitor element connected in series). In many electrochemical interfaces such as the IL-electrode interface, the double-layer capacitance may not strictly adhere to ideal capacitor behavior. The deviations from the ideal behavior stem from factors such as electrode roughness[93] and the sluggish nature of processes like ion adsorption, ion reorientation, and lateral reorganization of adsorbed ions on the electrode, as detected by time-resolved X-ray reflectivity (XRR).[94] Considering the distributed time constants introduced by these factors which result in non-ideality, the capacitance is more accurately represented by a constant phase element (CPE) in an equivalent circuit analysis rather than a capacitor. This way, CPE can also account for inertial motions and voltage-induced transformations of bulky or asymmetric ions of ILs and DESs, on the electrode surface. The capacitance of the corresponding R-CPE circuit can then be expressed as:

$$C = \frac{1}{n}\sum_i \left[\frac{Q\,\omega_i^{\alpha-1}}{\sin\left(\frac{\alpha\pi}{2}\right)}\right] \qquad \text{eqn (2)}$$

where 'Q' and 'a' are fit parameters; Q corresponding to the charge and 'a' corresponding to the deviation of CPE from ideal capacitor (a=1) whereas ω_I is the angular frequency (Hz).

Given that the potential-dependent characteristics of the differential capacitance provide crucial insights for comparing theory predictions with experimental data, it is highly advisable to collect EIS spectra across a wide-range of frequencies and conduct fitting of the spectra instead of relying solely on single-frequency calculations. To effectively fit the R-CPE circuit, it becomes crucial to discern the frequency range governing the charging and discharging of the double-layer, excluding other phenomena occurring during the formation of the double layer such as molecular reorientation and surface adsorption. The frequency of interest can be identified by transforming the Nyquist plots (Z' vs. Z") into complex capacitance plots (C' vs. C") using the equation 3, where the double layer formation manifest itself as a semi-circle on the C' vs. C" plot.[95]

$$C = C' + iC'' = \frac{1}{i\omega Z} = -\frac{iZ'}{\omega\,(Z'^2 + Z''^2)} - \frac{iZ''}{\omega\,(Z'^2 + Z''^2)} \qquad \text{eqn (3)}$$

C' and C" correspond to the real and imaginary components of capacitance, respectively, whereas Z' and Z" are the real and imaginary components of impedance, respectively. This analysis makes sure that only frequencies corresponding to the characteristic time for double-layer charging is used in the analysis.

The Goodwin-Kornyshev (GK) model has been applied to many early experimental works. Lockett et al.[96] examined $[BMIM]^+$ based ILs with various anions ($[BF_4]^-$, $[PF_6]^-$, and $[Cl]^-$) on different electrodes (Pt, Au and GC). The capacitance curves all displayed a camel-shape, but with different PZCs. They found that specific adsorption due to interactions between the electrode and the electrolyte components has an influence on the curve near the PZC. Jitvisate et al.[97] also observed camel-shaped differential capacitance curves in neat ILs, studying $[EMIM]^+$ with $[TFSI]^-$ and $[BF_4]^-$. The varying local maxima at the positive end of $[EMIM][BF_4]$ compared to [EMIM][TFSI], indicated the impact of ion size. In the case of $[EMIM][BF_4]$, the spherical anions were substantially smaller than the cations, resulting in a higher and steeper capacitance peak during the positive polarization. However, the agreement with the model for [EMIM][TFSI] was less pronounced, with similar local maxima for negative and positive ends due to comparable sizes of the anion and the cation. They noted that the GK model fit better with ILs having small-sized ions.

When examining capacitance, variables such as placement of electrodes for a uniform current distribution, the electrode roughness, and the potential scan direction (positive-to-negative *vs.* negative-to-positive) should be considered as hysteresis are known to occur. Capacitance hysteresis, characterized by a delayed respond to the applied potential, introduces difficulties in measurement and comparison of consecutively acquired data points. This complexity is elaborated in the study by Gore et al. [98] where EIS *vs.* linear AC voltammetry was shown to have an impact. Lockett et al. [96] found that scans starting from the OCP yield more consistent results, while Zhou et al.[99] highlighted the experimental challenges in returning to the initial OCP once potential is swept in once direction. Druschler et al.[100] investigated the differential capacitance behavior of [EMIM][TFSI] and [BMpyr][TFSI] on a $Pt_{(poly)}$ electrode using broadband EIS. They observed capacitive hysteresis dependent on scan direction, attributing it to slow pseudo-capacitive processes, likely tied to ion adsorption at frequencies below 10 Hz. To understand the structural origins of the capacitive hysteresis, Uysal et al.[101] employed X-ray reflectivity (XR) and MD simulations to graphene-$[C_9mim][TFSI]$ interface. They attributed the slow response of interfacial structure to applied potential due to steric hindrance and scan-direction-dependent hysteresis to the reorganization of alternating anion and cations layers seen in XR.

Efforts to mitigate hysteresis and ensure consistent interface probing by EIS have been explored by Lucio and Shaw.[102] Alternatively, Luco et al.[103] introduced the large-amplitude (50-200 mV) Fourier-transformed AC voltammetry (FT-ACV) technique that employed frequency range of 10 Hz to 1 kHz with single frequency perturbations. This method overcame scan-direction dependent hysteresis. Another study by Lucio et al.[104] using FT-ACV method focused on the interface of boron-doped diamond (BDD) electrodes with various ILs where nearly ideal capacitive behavior was obtained without any impact from IL composition or scan direction. We believe this result is likely due to the very inert behavior of the BDD electrode.

Our group examined the differential capacitance of a series of ILs with $[N_{1114}]^+$, $[EMIM]^+$, and $[PYR_{13}]^+$ cations and $[TFSI]^-$ anion on GC electrode.[105] **Figure 5a** shows the measured differential capacitance curves as a function of applied potential, where only camel-shaped curves were obtained. The capacitance behavior around PZC (data in hollow symbols) aligns with the predictions of GK theory (fitted solid line). However, the decay past the maxima in both negative and positive potential sweep deviate from the theoretical expectations. When contrasting theoretical predictions with the experimental data, it becomes apparent that the potential-dependent attributes of the experimental findings are more broader than the theoretical predictions. The XRR investigations uncovered the presence of three different time scales linked to ionic rearrangements on the electrode surface.[94] These timescales include the vertical movement of ions, taking place within 1-10 milliseconds, and the reorientation and lateral ordering of molecules, which occur over a longer period of 10-100 milliseconds. As a result, the discrepancy between the theory and the experimental data in **Figure 5a** arises because the theoretical models fail to incorporate non-Coulombic interactions between ions and surface atoms, as well as slower processes occurring such as ion reorientations and specific ion adsorption. The necessity to screen the surface charge on the electrode with more counter-ions in the electrolyte at higher potentials crowds the interface. However, ion reorganize at the electrode surface intuitively gets more difficult as the surface gets more crowded.

What is interesting in the capacitances shown in **Figure 5a** is the asymmetry in the camel-shaped curves. In particular, for $[PYR_{13}][TFSI]$ and [EMIM][TFSI], a higher increase in capacitance upon positive polarization is seen even though the anion is the same, compared to negative polarization. With positive polarization of the electrode, it is expected

that the anions will enrich the interface. However, despite the fact that all of the ILs have the same $[TFSI]^-$ anion, the excess charge density seems to be different. This suggests that the cation also plays a crucial role in determining excess anion packing due to significant ionic interactions, leading to differences in the absolute values of maxima in differential capacitances. This is more clearly seen in **Figure 5b** where ILs with $[TFSI]^-$ anion and quaternary ammonium cations with varied alkyl chain length and ether functionality were examined; it shows a greater extend of increase in capacitance for $[N_{1888}][TFSI]$ (comparing global maxima with PZC capacitances)[106]. The ammonium ILs have a slightly wider electrochemical stability compared to those with $[PYR_{13}]^+$ and $[EMIM]^+$, in particular, extending the positive limit towards 3 V (vs. Fc/Fc^+) on GC. With the increased flexibility induced by the longer alkyl chains and ether linkage (i.e., $[N_{122(201)}]$), the quaternary cation intrudes into the anion-rich layers of the interface resulting in increased compacity and increased capacitive storage but also faster decay past the maxima due to the increased interfacial thickness. Complementary SERS analysis, albeit on silver electrode, suggested the compaction and reduced rotational freedom for the quaternary ammonium cation, $[N_{1888}]^+$, with increased polarization.[106] When the surface charge was increasingly positive, the intruding alkyl chains of the cation prevented anion-anion repulsions, thus resulting in increased capacitance. On the other hand, the chains buckled upon increased negative polarization, thus enabling more ion accommodation, and again increasing the capacitance with respect to PZC. However, the increase upon negative polarization was not as significant due to large size of $[N_{1888}]^+$ cation that thickens the double layer without a substantial increase in excess charge. As seen from the fits of GK model to the measured data in **Figure 5**, the mean field theory presents a fairly good description of the IL-electrode interface especially with non-reactive electrodes such as GC. Further, it is agreed that the molecular-level arrangement of ILs at an electrified surface is influenced by the ion size, functional moieties, and the lengths of the alkyl chain subsitutions.[107]

Unlike ILs, we found that the GK model does not work well or not needed for DESs despite their similarity to ILs. In ionic DESs such as ethaline, the halide salt is dissociated to some degree by hydrogen bonding with the HBD component (e.g., $EG\text{-}Cl^-$ and $EG\text{-}Ch^+$); in turn the ions also present hydrogen bonding (i.e., between -OH of Ch^+ and Cl^-). Therefore, the solvated ions present minor capacitance variations upon varied potential as attributable to steric constraints. As a result, the capacitance curves do not have many features in the absence of specific ion adsorption (**Figure 3**). On more reactive electrodes such as Pt, the electrochemical stability window is also narrower and virtually no change in ion density is captured by EIS, while on GC electrode with wider negative limit, a capacitance curve resembling a shallow U-shape emerged. This is better seen in **Figure 6a** where $[TFSI]^-$, weakly coordinating ion, was replaced with Cl^- in ethaline; blue triangles represent a U-shape. However, the increase in capacitance with potential does not match with that of neither Gouy-Chapman nor Goodwin-Kornyshev descriptions. Therefore, Dean et al.[21] proposed a modified Gouy-Chapman model to describe DES-electrode interfaces:

$$C_{GC} = C_d \cosh(\alpha\, u/2) \qquad \text{eqn (4)}$$

where α is the new interaction parameter to account for the hydrogen bonding and ionic interactions in DESs, C_d is Debye capacitance and controlled by Debye length, and u is dimensionless potential, as defined before.

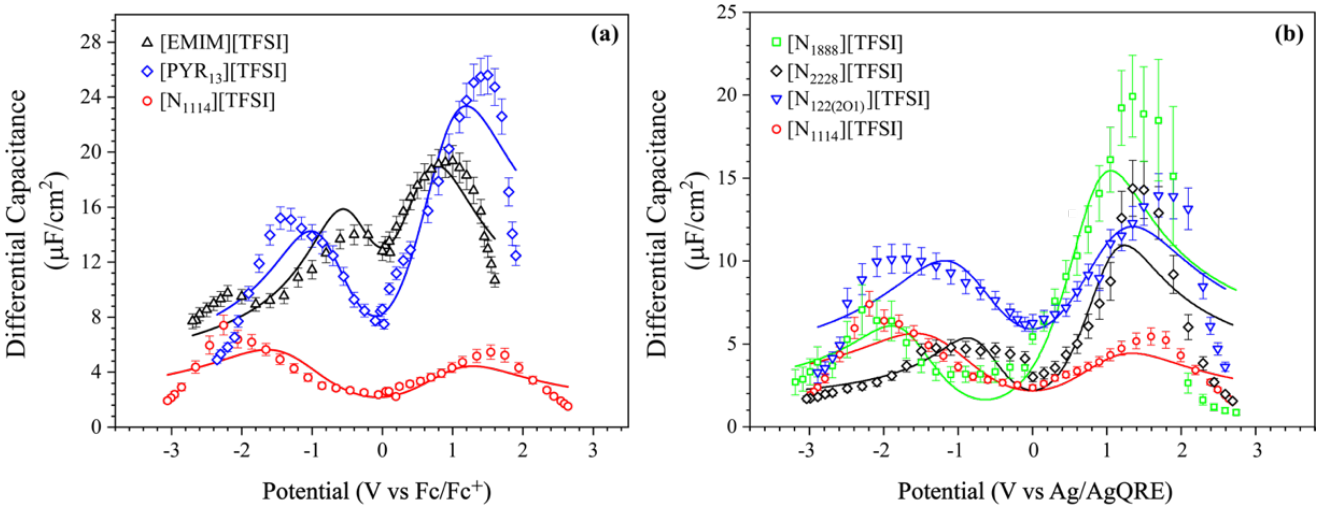

Figure 5. (a) Differential capacitance of [EMIM][TFSI], $[PYR_{13}][TFSI]$, and $[N_{1114}][TFSI]$ on a GC electrode. Reprinted with permission from ref. 105. Copyright 2019 Royal Society of Chemistry, (b) Differential capacitance of $[N_{1888}]$, $[N_{2228}]$,$[N_{122(201)}]$ and $[N_{1114}]$ cations of different alkyl chain length with [TFSI] anion. Reprinted with permission from ref. 106. Copyright 2019 American Chemical Society. EIS was conducted within the frequency range of 500 kHz- 100 mHz, with an amplitude of 10 mV. The lines are the fits with the mean-field model of Goodwin–Kornyshev. Error bars indicate the statistical average associated with averaged capacitance values calculated in the range of frequencies with a 90% confidence interval.

Accounting for the interactions through α fit the data well as seen from the solid lines in **Figure 6a**. The evaluated α varied between 0.011 for ChCl:EG (1:2) and 0.012 for 1:4, 1:6, and 1:20 mixtures, which demonstrates significant

deviation from dilute electrolytes (α would be 1 for completely dissociated salts) and no dependence on the HBA:HBD ratio since hydrogen bonding is present at all compositions. In comparison, the equivalent ion-ion interaction parameter in the GK model for ILs ranged between 0.02 and 0.12,[105, 106] presenting larger deviations from the dilute system in comparison to ChCl:EG mixtures. To further investigate on the impact of ion charge density and the strength of hydrogen bonding on capacitance curves, Dean et al.[108] examined mixtures of choline acetate (ChAc) and choline oxalate (Ch_2Ox) in comparison to ChTFSI and ChCl; all with EG at molar ratios of 1:2 and 1:4. The strength of the hydrogen bonding network was shown to vary with the ion charge density as examined in the bulk liquid through the examination of physical properties, NMR, and the energies calculated for representative clusters of anion-EG solvated ions by density functional theory.

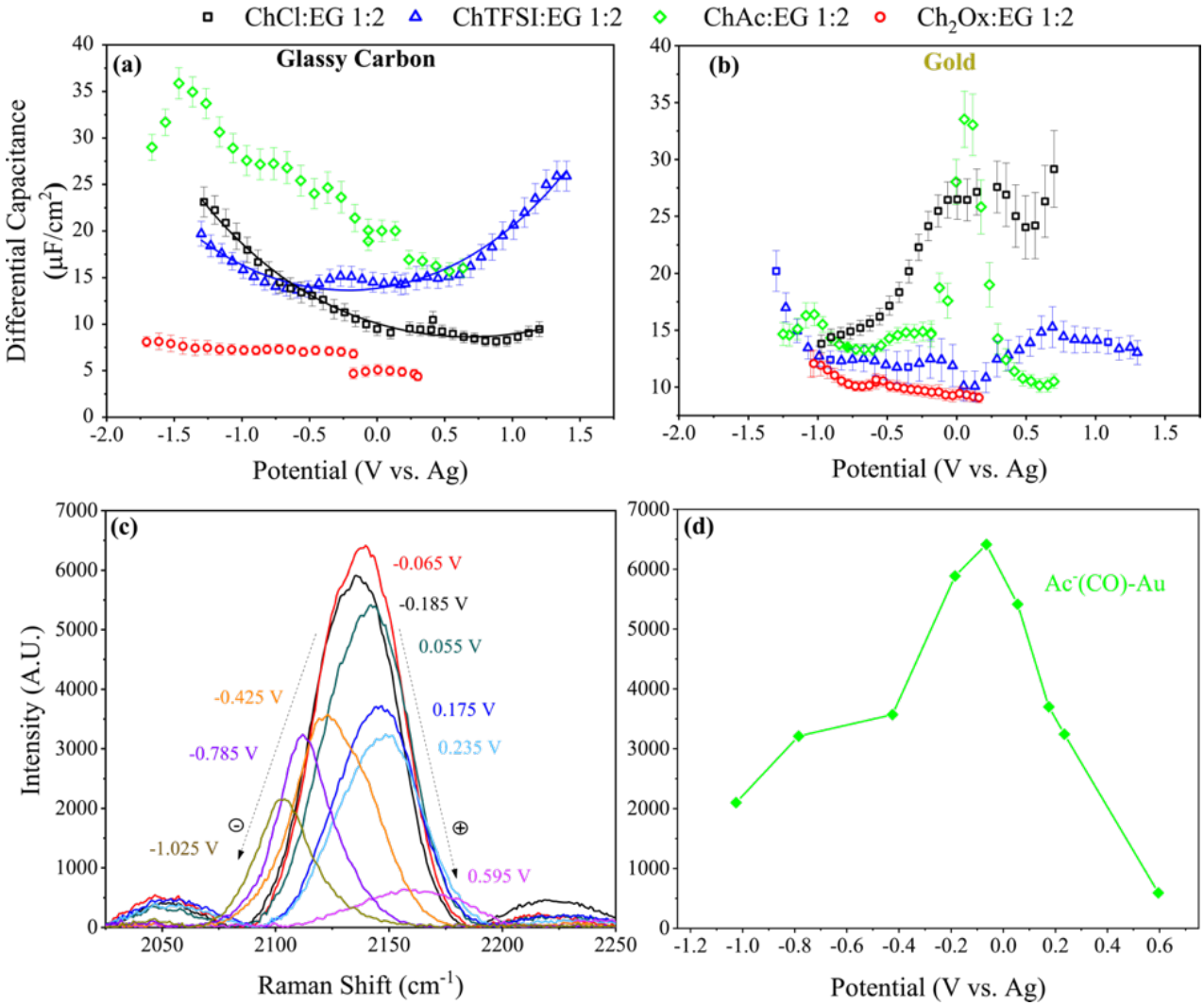

Figure 6. Differential capacitance curves for ChCl:EG, ChTFSI:EG, ChAc:EG and Ch_2Ox:EG (1:2) mixtures on GC (a) and Au (b) electrodes. Solid lines indicate the modified Gouy-Chapman fits. EIS was conducted within the frequency range of 500 kHz to 100 mHz with an amplitude of 20 mV. Localized surface-enhanced Raman spectroscopy of choline ChAc:EG (1:2) (c) at select potentials on a roughened Au electrode with a 785 nm excitation laser at a spectral range of 600 to 2300 cm^{-1} with a 20x magnification objective and the peak intensity of -CO moiety of surface adsorbed $[Ac]^-$ (d) indicating Au-$[Ac]^-$ interactions. Reprinted with permission from ref. 108. Copyright 2022 American Chemical Society.

This bulk property was found to impact the interfacial behavior. EIS and SERS analysis probing the interface on GC (**Figure 6a**) and Au (**Figure 6b**) electrodes revealed a contrasting behavior between Ac^- (green) and Ox^{2-} (red) systems despite their structural similarities. For ChAc:EG on GC electrode, there was a steady increase in capacitance upon negative polarization demonstrating the responsiveness in Ch^+ ions while virtually no change was observed for Ch_2Ox:EG. On Au electrode, the electrochemical stability window was narrower for both and the PZC capacitance was lower for Ch_2OX:EG, compared with GC. Further, the potential-dependence was nearly absent for Ch_2Ox:EG on Au, similar to GC. The strong association between Ox^{2-} anions and EG molecules restricts the ion mobility and restructuring, whereas for Ac^-, de-solvation and surface adsorption occurred, as evidenced by the peak appearance in capacitance

(**Figure 6b**) and the increase in peak intensity in SERS for Ac^- (**Figure 6c**). Compared to ChCl:EG where Cl^- adsorption was previously reported (**Figure 3**),[21] this behavior in capacitance is similar. SERS peak intensity for the -CO moiety of Ac^- (**Figure 6d**) follows a very similar trend to that of the capacitance curve (**Figure 6b**), thus providing evidence to the surface adsorption of Ac^- (not present in SERS of Ch_2OX:EG). ChTFSI:EG system displayed a dampened U-shaped differential capacitance on both GC and Au electrodes; the nearly identical capacitance on both surfaces suggests that anion surface adsorption is not a concern. It can be concluded that for DESs with strong hydrogen bonding interactions, the interfacial charge density is not a strong function of the applied potential within the limited electrochemical stability window due the inability to these systems to efficiently screen the surface charge. On the other hand, specific ion adsorption can occur, leading to deviations from the modified Gouy-Chapman model.

SIGNIFICANCE OF THE ELECTRODE-ELECTROLYTE INTERFACE IN ENERGY STORAGE AND CONVERSION

The interfacial structure significantly influences the voltage profile hence the thermodynamics and kinetics of electrochemical reactions (e.g., in energy storage devices,[109] sensors,[110] and electrocatalytic reactors[111]). In particular, a direct connection can be made between the capacitance and the energy storage capacity, eqn. 5, in electrical double layer capacitors, also known as supercapacitors.

$$C = \frac{q}{V} \qquad \text{eqn (5)}$$

C is the capacitance, q is charge, and V is voltage applied.

In supercapacitors, the fundamental charging/discharging process relies on the electrosorption of ions from an electrolyte onto electrode surface under an applied electric potential.[112] As seen in equation 5, excess ion accumulation and the charge density are important measures. These parameters can be directly probed with the differential capacitance analysis discussed previously. However, real capacitors employ porous electrodes for an increased electrode-electrolyte surface area.[113] Therefore, additional parameters like electrode wettability,[114, 115] electrode materials and structure,[116] electrolyte composition,[117] and electrode-electrolyte compatibility[118] needs to be considered. There has been a body of work from Gogotsi and colleagues examining ion adsorption on carbonaceous electrodes and ion accumulation in porous and structured carbons.[119-121] These contributions have clarified the mechanisms of diffusion, electrosorption, aggregation, dynamics, the resulting electrochemical behavior,[121] and the capacitive performance[122] of ILs inside porous carbon and related nanostructured electrodes with complex pore architectures and surface chemistries. Moreover, double layer formation and voltage-induced structural reconfigurations in these complex electrodes are still harder to predict in the case of ILs where pore sizes reach down to ion sizes; ions are further asymmetric and their accessibility into and mobility within the pores may depend on the ion reorientations. There has been interest in DESs as supercapacitor electrolytes due to electrochemical stability, lack of flammability, and scalable availability, as alternatives to ILs.[123] While many reports document their practicality, the fundamental research and theoretical work on the DES-electrode interface on both flat and porous electrodes is needed to enable DES design for improved supercapacitors. For a thorough examination of the theory and simulations regarding ILs in nanoconfinement, readers are encouraged to consult the perspective article authored by Perkin [124] and a more recent in-depth review provided by Kondrat et al.[125]

The electrode-electrolyte interfacial structure has an influence on nucleation and film growth during electrodeposition processes. The use of ILs and DESs in metal electrodeposition has piqued significant interest, aiming to tackle some of the challenges linked with electroplating in aqueous electrolytes. These challenges include low current efficiency and the complexity of bath formulations. In particular ILs and DESs enable the deposition of reactive metals[126] and metal-alloys[127] that are typically challenging to obtain in aqueous solutions due to electrochemical stability and solubility limitations. Abbott et al. [128] conducted a comparative study on nickel (Ni) deposition in ethaline DES and a Watts bath (a commonly used aqueous electrolyte for Ni deposition). The Ni layer deposited from the DES exhibited uniform density, resulting in a smooth, featureless, and highly reflective surface. In contrast, the Ni layer obtained from the Watts bath showed a rougher surface with a dull appearance. Additionally, the Ni layer obtained from the DES was notably harder than that from the Watts bath, indicating a finer grain size for Ni deposits from the DES electrolyte. Moreover, ILs featuring bulky cations tend to result in more smaller structures, opening up possibilities for various nanoscale depositions[129], with potential applications in fabrication of sensors.[130] Due to the ability to tune metal speciation[131] and therefore the redox potentials, ILs are found advantageous for deposition of various metals such as aluminum (Al)[132] and rare earth metals,[133] with impactful applications such as the fabrication of semiconductors.[134] Even though the mechanistic understanding of how the individual ions in ILs control the deposition process is not yet fully developed,[135] ILs present significant impact on deposit morphology, attributed to their unique interfacial structuring, in some cases their specific adsorption, and ultimately their influence on the charge transfer kinetics through speciation that differ from conventional electrolytes.

Measuring reaction kinetic parameters in IL and DES electrolytes using traditional electrochemical techniques is challenging due to the mass transfer limitations imposed by these viscous liquids. In particular, the conventional Tafel analysis is not appropriate since the limiting current in ILs and DESs are too small in order to obtain a linear Tafel slope where the increase in potential directly correlates with increase in current. For example, by employing Tafel analysis, Shaheen et al.,[136] calculated a charge transfer coefficient of 0.9 for the oxidation of the redox-active molecule (2,2,6,6-trimethylpiperidin-1-yl)oxyl (TEMPO) in ethaline, demonstrating a significant deviation from the expected value of 0.5 for a single electron transfer reaction. Later, this was explained through the surface adsorption of oxidized TEMPO, as evident in SERS analysis we performed.[137] The oxidized TEMPO desorbs from the surface at a much slower rate than the molecular diffusion rate and the electron transfer rate. This was in fact found to be the case even in aqueous media. Nonetheless, Savinell, Wainright, and colleagues[23] reported that Tafel analysis works well when the exchange current density is less than the 57% of the limiting current. Therefore, for electrolytes where the limiting current is already

very small, they developed an extended Butler-Volmer equation in order to study electrokinetics in DESs for estimating accurate exchange current density and transfer coefficients. Such methods are especially useful considering the various applications of ILs and DES where reaction rates are important such as redox flow batteries (RFBs) employing high energy density electrolytes.

RFBs utilize flowing electrolytes and redox reactions for energy storage; hence the adsorbed species at the electrode surface and overpotentials induced by viscous DESs can significantly influence the kinetics of charge transfer in these systems. DESs have been found particular interesting for RFBs due to their low volatility and high concentrations of redox active species. Since the energy density is related to the concentration of active material, cell voltage, and the number of electrons transferred during the redox reaction, the use of DESs such as ethaline can help increase the solubility limit and facilitate the electron transfer reactions. While TEMPO redox is shown to be unstable in ethaline due to side reactions[138] in addition to the surface adsorption phenomenon, viologens have shown promise, in particular due to accessibility of the second electron transfer as first reported by Klein et al.,[139] a process unattainable in aqueous electrolytes. In our follow-up study, Ghahremani et al.[140] further examined this chemistry to evaluate their suitability for RFB applications. The SERS investigation uncovered that when the surface remains at open circuit potential, an inner layer forms comprising the Ch^+ and EG, effectively shielding the dicationic MV^{+2} from the surface. Upon the application of a negative potential, the emergence of ring modes characteristic of the viologen indicates the presence of $MV^{+\bullet}$ (also confirmed by the distinct blue color of this radical), accompanied by a decline in the intensity of peaks related to Ch^+ and EG. However, following the relaxation of potential, $MV^{+\bullet}$ continues to persist on the surface, while the peaks for Ch^+ and EG remain suppressed. This persistence of peaks underscores the enduring presence of $MV^{+\bullet}$, indicating a desorption-limited behavior, a phenomenon also observed for TEMPO.[137] The slow desorption of $MV^{+\bullet}$ impacts the kinetics of the oxidation-reduction reaction. This can restrict the rate of electron transfer and charge exchange, affecting overall efficiency and reaction rate. Additionally, the inner layer of $MV^{+\bullet}$ on the electrode surface can obstruct electroactive sites, partially or fully occupying them. This limits the availability of these sites for the charge transfer process, further reducing the reaction rate and overall efficiency. To enhance desorption rates and address these issues, strategies such as modifying the electrode material or adjusting electrochemical conditions can improve the performance of RFBs.[141] Understanding and managing the electroactive species in the inner-most layer are crucial for optimizing the efficiency of the electrode and ensuring reliable energy storage and conversion in RFBs.

Electrocatalysis is yet another domain where the interfacial structure is crucial to understand such as the case for the electrochemical CO_2 reduction reaction (CO_2RR).[142] In particular, ILs and DESs are known for their high CO_2 solubility,[143-145] thus present advantages compared to the aqueous electrolytes with low CO_2 solubilities.[146] The $[EMIM][BF_4]$ IL was even reported to co-catalyze the CO_2RR.[147] Additionally, ILs can suppress the hydrogen evolution reaction (HER), a competing side reaction in aqueous electrolytes. In relation to the role of ILs on catalyzing the CO_2RR, it has been proposed that ILs create a unique structural arrangement near the electrode surface, playing a stabilizing role for the adsorbed high-energy intermediates like $CO_2^{-\bullet}$.[148] Sum frequency generation (SFG) was employed to study CO adsorption at the $[EMIM][BF_4]$-Pt interface to specifically examine the double-layer structure, finding the interface comprises a Helmholtz-like one ion thick layer.[149] Subsequent research employing surface tunneling microscopy (STM) indicated that the ordering of ILs near the electrode may involve either the monolayer formation or a few multilayers comprising alternating counter- and co-ions, depending on the potential.[150, 151] This points to the possibility that IL double-layers at electrode surfaces may undergo potential-dependent transitions, and these structural changes, primarily induced by negative potentials under reductive conditions such as parallel alignment of imidazolium cations to the surface,[152] can have ramifications for the cation adsorption and the electric field strength, and further have been linked to co-catalytic activity of ILs for CO_2RR.[153]

While earlier investigations of IL electrolytes for CO_2RR primarily focuses on physisorbing ILs, the development of functionalized ILs has introduced a more intricate dynamics that extends beyond the transportation of neutral dissolved CO_2 to the electrode surface, and its interaction with the microenvironment formed by IL, and shifts focus to the species bound to CO_2 and their behavior at the electrode surface. This shift underscores the necessity of comprehensively understanding the mechanisms of CO_2 binding and the processes away from the equilibrium as dynamic nature of the interface presents electron transfer reaction in parallel to other chemical reactions such as hydrogen transfer among the IL ions, and CO_2 chemisorption by both the anion and the cation. Recently, we reported on the reduction of the onset potential of CO_2RR on Ag[154] and Cu[155] electrodes with a CO_2-reactive [EMIM][2-CNpyr] IL in non-aqueous electrolyte where the microenvironment and the catalytic role of the IL was examined through the interfacial structure and surface species as investigated by EIS and in-situ SERS. While CO was obtained as the only product over Ag (> 95% Faradic efficiency), various C_{2+} products were reported over Cu owing to the stabilization of the reaction intermediates on the electrode surface and the hydrogen bonding among the interfacial species. Speciation at the electrode surface due to chemisorption and the dynamic microenvironment created by the reactive ILs presents new advances towards controlling electrocatalytic reaction outcomes. To better understand and control these reactive interfaces, there are new questions that need to be answered: (1) How do the in-situ formed species from CO_2 chemisorption contribute to the overall electrochemical environment?; (2) How do double layer structuring differ from those encountered in conventional (physisorbing) ILs?; (3) What aspects of the microenvironment control the thermodynamics and electrokinetics? To answer these questions, the simultaneous application of advanced spectroscopy and electroanalytic techniques is required. Further, the interpretation of the experimental data should be strengthened by computational studies from atomistic to macro scale.

OUTLOOK

Significant progress has been made in understanding the interfacial electrochemistry of concentrated electrolytes ILs

and DESs, with researchers combining spectroscopic and electrochemical techniques to explore the potential-dependent behavior of the interface. However, a comprehensive understanding of the double-layer structure is still needed, and the choice of concentrated electrolyte presents a challenge in establishing a generalized understanding while allowing customization for desired interfacial properties. Anion size, ion charge density, and ion-electrode interactions are crucial in ion packing, dynamics, and interfacial behavior in hydrogen-bonded electrolytes with high salt concentrations. A more precise understanding of the interface will undoubtedly contribute to our comprehension of electrode reactions. Currently available theories represent significant advancements towards describing the profiles of differential capacitance curves by considering ion size differences, short-range interactions, and ionic dielectric properties. However, these theories fail to explain the oscillations observed in local species concentrations and does not capture universally the behavior of DESs, in particular. Another major challenge lies in explicitly addressing the behavior of electrons at the metal electrode. Furthermore, as ILs and DESs are hygroscopic solvents, influence of water on differential capacitance and electrochemical reactions is crucial to consider. By further investigating the complexities of electrolyte-electrode interfaces, new possibilities for designing advanced electrochemical devices based on functionalized IL and DES electrolytes with enhanced performance and efficiency can be possible for targeted electrochemical applications.

CONCLUSION

In conclusion, recent research efforts have significantly advanced our understanding of the interfacial electrochemistry of concentrated electrolytes such as ILs and DESs, where in-situ spectroscopic, reflectivity, and electrochemical techniques have been instrumental in probing the structure and potential-dependent behavior of these interfaces. Continued research is essential to unlock the full potential of concentrated electrolytes to take advantage of tailorable polarity, wide electrochemical stability, high solubility of redox species, and low volatility and to enable the design of advanced electrochemical systems based on concentrated electrolytes with enhanced performances.

AUTHOR INFORMATION

Corresponding Author

Burcu Gurkan – Chemical and Biomolecular Engineering, Case Western Reserve University, Cleveland, Ohio 44106, United States; orcid.org/0000-0003-4886-3350; e-mail: beg23@case.edu

Acknowledgements

This study was funded by an NSF CAREER award (no. 2045111) from the Division of Chemical, Bioengineering, Environmental and Transport Systems (CBET), Interfacial Engineering, and Electrochemical System. Authors acknowledge partial support from Breakthrough Electrolytes for Energy Storage (BEES)—an Energy Frontier Research Center (EFRC) of the U.S. Department of Energy, Office of Science, Basic Energy Sciences under Award # DE-SC0019409 and Center for Closing the Carbon Cycle (4C) EFRC, under Award # DE-SC0023427.

REFERENCES

(1) Bockris, J.; Reddy, A.; Gamboa-Aldeco, M. Modern Electrochemistry. Second edn, Vol. 2A. Kluwer Academic/Plenum Publishers: 2000.

(2) Schmickler, W. Double layer theory. *Journal of Solid State Electrochemistry* **2020**, *24*, 2175-2176.

(3) Luque, N. B.; Woelki, S.; Henderson, D.; Schmickler, W. A model for the electrical double layer combining integral equation techniques with quantum density functional theory. *Electrochimica acta* **2011**, *56* (21), 7298-7302.

(4) Mountain, R. D. Solvation structure of ions in water. *International journal of thermophysics* **2007**, *28*, 536-543.

(5) Helmholtz, H. About some laws of the distribution of electrical currents in physical conductors, with application to animalelectrical experiments (conclusion). *Ann. Phys* **1853**, *165*, 353-377.

(6) Chapman, D. Diffuse Distribution of Adsorbed Ions. *Phil. Mag* **1913**, *25*, 475.

(7) Stern, O. Zur theorie der elektrolytischen doppelschicht. *Zeitschrift für Elektrochemie und angewandte physikalische Chemie* **1924**, *30* (21-22), 508-516.

(8) Ficke, L. E.; Brennecke, J. F. Interactions of ionic liquids and water. *The Journal of Physical Chemistry B* **2010**, *114* (32), 10496-10501.

(9) Crowhurst, L.; Mawdsley, P. R.; Perez-Arlandis, J. M.; Salter, P. A.; Welton, T. Solvent–solute interactions in ionic liquids. *Physical Chemistry Chemical Physics* **2003**, *5* (13), 2790-2794.

(10) Zhang, S.; Wang, J.; Lu, X.; Zhou, Q. *Structures and interactions of ionic liquids*; Springer, 2013.

(11) Baldelli, S. Surface Structure at the Ionic Liquid−Electrified Metal Interface. *Accounts of Chemical Research* **2008**, *41* (3), 421-431. DOI: 10.1021/ar700185h.

(12) Santos, C. S.; Baldelli, S. Surface Orientation of 1-Methyl-, 1-Ethyl-, and 1-Butyl-3-methylimidazolium Methyl Sulfate as Probed by Sum-Frequency Generation Vibrational Spectroscopy. *The Journal of Physical Chemistry B* **2007**, *111* (18), 4715-4723. DOI: 10.1021/jp067056l.

(13) Wilkes, J. S. A short history of ionic liquids—from molten salts to neoteric solvents. *Green Chemistry* **2002**, *4* (2), 73-80, 10.1039/B110838G. DOI: 10.1039/B110838G.

(14) Smith, E. L.; Abbott, A. P.; Ryder, K. S. Deep Eutectic Solvents (DESs) and Their Applications. *Chemical Reviews* **2014**, *114* (21), 11060-11082. DOI: 10.1021/cr300162p.

(15) Abbott, A. P.; Boothby, D.; Capper, G.; Davies, D. L.; Rasheed, R. K. Deep Eutectic Solvents Formed between Choline Chloride and Carboxylic Acids: Versatile Alternatives to Ionic Liquids. *Journal of the American Chemical Society* **2004**, *126* (29), 9142-9147. DOI: 10.1021/ja048266j.

(16) Abranches, D. O.; Coutinho, J. A. P. Everything You Wanted to Know about Deep Eutectic Solvents but Were Afraid to Be Told. *Annual Review of Chemical and Biomolecular Engineering* **2023**, *14* (1), 141-163. DOI: 10.1146/annurev-chembioeng-101121-085323.

(17) Hansen, B. B.; Spittle, S.; Chen, B.; Poe, D.; Zhang, Y.; Klein, J. M.; Horton, A.; Adhikari, L.; Zelovich, T.; Doherty, B. W.; et al. Deep Eutectic Solvents: A Review of Fundamentals and Applications. *Chemical Reviews* **2021**, *121* (3), 1232-1285. DOI: 10.1021/acs.chemrev.0c00385.

(18) Fedorov, M. V.; Kornyshev, A. A. Ionic Liquids at Electrified Interfaces. *Chemical Reviews* **2014**, *114* (5), 2978-3036. DOI: 10.1021/cr400374x.

(19) de Souza, J. P.; Goodwin, Z. A. H.; McEldrew, M.; Kornyshev, A. A.; Bazant, M. Z. Interfacial Layering in the Electric Double Layer of Ionic Liquids. *Physical Review Letters* **2020**, *125* (11), 116001. DOI: 10.1103/PhysRevLett.125.116001.

(20) Shen, D.; Steinberg, K.; Akolkar, R. Avoiding Pitfalls in the Determination of Reliable Electrochemical Kinetics Parameters for the Cu2+ → Cu1+ Reduction Reaction in Deep Eutectic Solvents. *Journal of The Electrochemical Society* **2018**, *165* (14), E808. DOI: 10.1149/2.1011814jes.

(21) Dean, W.; Klein, J.; Gurkan, B. Do Deep Eutectic Solvents Behave Like Ionic Liquid Electrolytes? A Perspective from the Electrode-Electrolyte Interface. *Journal of The Electrochemical Society* **2021**, *168* (2), 026503. DOI: 10.1149/1945-7111/abde83.

(22) Shen, X.; Sinclair, N.; Wainright, J.; Akolkar, R.; Savinell, R. F. Evaluating and Developing a Reliable Reference Electrode for Choline Chloride Based Deep Eutectic Solvents. *Journal of The Electrochemical Society* **2020**, *167* (8), 086509. DOI: 10.1149/1945-7111/ab913c.

(23) Shen, X.; Sinclair, N.; Wainright, J.; Savinell, R. Methods—Analyzing Electrochemical Kinetic Parameters in Deep Eutectic Solvents Using an Extended Butler-Volmer Equation. *Journal of The Electrochemical Society* **2021**, *168* (5), 056520.

(24) Buchner, F.; Forster-Tonigold, K.; Uhl, B.; Alwast, D.; Wagner, N.; Farkhondeh, H.; Gross, A.; Behm, R. J. Toward the microscopic identification of anions and cations at the ionic liquid| Ag (111) interface: a combined experimental and theoretical investigation. *ACS nano* **2013**, *7* (9), 7773-7784.

(25) Waldmann, T.; Huang, H. H.; Hoster, H. E.; Höfft, O.; Endres, F.; Behm, R. J. Imaging an ionic liquid adlayer by scanning tunneling microscopy at the solid| vacuum interface. *ChemPhysChem* **2011**, *12* (14), 2565-2567.

(26) Richey, F. W.; Dyatkin, B.; Gogotsi, Y.; Elabd, Y. A. Ion dynamics in porous carbon electrodes in supercapacitors using in situ infrared spectroelectrochemistry. *Journal of the american chemical society* **2013**, *135* (34), 12818-12826.

(27) Motobayashi, K.; Minami, K.; Nishi, N.; Sakka, T.; Osawa, M. Hysteresis of potential-dependent changes in ion density and structure of an ionic liquid on a gold electrode: in situ observation by surface-enhanced infrared absorption spectroscopy. *The Journal of Physical Chemistry Letters* **2013**, *4* (18), 3110-3114.

(28) Zhang, M.; Yu, L.-J.; Huang, Y.-F.; Yan, J.-W.; Liu, G.-K.; Wu, D.-Y.; Tian, Z.-Q.; Mao, B.-W. Extending the shell-isolated nanoparticle-enhanced Raman spectroscopy approach to interfacial ionic liquids at single crystal electrode surfaces. *Chemical Communications* **2014**, *50* (94), 14740-14743.

(29) Zhang, N.; Wang, X.-R.; Yuan, Y.-X.; Wang, H.-F.; Xu, M.-M.; Ren, Z.-G.; Yao, J.-L.; Gu, R.-A. Probing double layer structure at Au/[BMIm]BF4 interface by molecular length-dependent SERS Stark effect. *Journal of Electroanalytical Chemistry* **2015**, *751*, 137-143. DOI: https://doi.org/10.1016/j.jelechem.2015.05.041.

(30) Santos, V. O.; Alves, M. B.; Carvalho, M. S.; Suarez, P. A. Z.; Rubim, J. C. Surface-Enhanced Raman Scattering at the Silver Electrode/Ionic Liquid (BMIPF6) Interface. *The Journal of Physical Chemistry B* **2006**, *110* (41), 20379-20385. DOI: 10.1021/jp0643348.

(31) Perera, G. S.; Nettles, C. B., II; Zhou, Y.; Zou, S.; Hollis, T. K.; Zhang, D. Direct Observation of Ion Pairing at the Liquid/Solid Interfaces by Surface Enhanced Raman Spectroscopy. *Langmuir* **2015**, *31* (33), 8998-9005. DOI: 10.1021/acs.langmuir.5b01903.

(32) Baldelli, S. Probing Electric Fields at the Ionic Liquid−Electrode Interface Using Sum Frequency Generation Spectroscopy and Electrochemistry. *The Journal of Physical Chemistry B* **2005**, *109* (27), 13049-13051. DOI: 10.1021/jp052913r.

(33) Bozzini, B.; Bund, A.; Busson, B.; Humbert, C.; Ispas, A.; Mele, C.; Tadjeddine, A. An SFG/DFG investigation of CN− adsorption at an Au electrode in 1-butyl-1-methyl-pyrrolidinium bis(trifluoromethylsulfonyl) amide ionic liquid. *Electrochemistry Communications* **2010**, *12* (1), 56-60. DOI: https://doi.org/10.1016/j.elecom.2009.10.035.

(34) Rivera-Rubero, S.; Baldelli, S. Surface Spectroscopy of Room-temperature Ionic Liquids on a Platinum Electrode: A Sum Frequency Generation Study. *The Journal of Physical Chemistry B* **2004**, *108* (39), 15133-15140. DOI: 10.1021/jp048260g.

(35) Klein, J. M.; Wang, H.; Sacci, R. L.; Browning, J. F.; Gurkan, B. Smooth modified surfaces of silicon for the study of ionic liquid interfaces by neutron reflectometry. *ACS Applied Electronic Materials* **2022**, *4* (5), 2217-2226.

(36) Budkov, Y. A.; Kolesnikov, A. L. Electric double layer theory for room temperature ionic liquids on charged electrodes: Milestones and prospects. *Current Opinion in Electrochemistry* **2022**, *33*, 100931. DOI: https://doi.org/10.1016/j.coelec.2021.100931.

(37) Li, C.-Y.; Le, J.-B.; Wang, Y.-H.; Chen, S.; Yang, Z.-L.; Li, J.-F.; Cheng, J.; Tian, Z.-Q. In situ probing electrified interfacial water structures at atomically flat surfaces. *Nature Materials* **2019**, *18* (7), 697-701. DOI: 10.1038/s41563-019-0356-x.

(38) Gonella, G.; Backus, E. H. G.; Nagata, Y.; Bonthuis, D. J.; Loche, P.; Schlaich, A.; Netz, R. R.; Kühnle, A.; McCrum, I. T.; Koper, M. T. M.; et al. Water at charged interfaces. *Nature Reviews Chemistry* **2021**, *5* (7), 466-485. DOI: 10.1038/s41570-021-00293-2.

(39) Conway, B.; Bockris, J. M.; Ammar, I. The dielectric constant of the solution in the diffuse and Helmholtz double layers at a charged interface in aqueous solution. *Transactions of the Faraday Society* **1951**, *47*, 756-766.

(40) Bockris, J. M.; Devanathan, M.; Müller, K. On the structure of charged interfaces. In *Electrochemistry*, Elsevier, 1965; pp 832-863.

(41) Grahame, D. C. Differential Capacity of Mercury in Aqueous Sodium Fluoride Solutions. I. Effect of Concentration at 25°. *Journal of the American Chemical Society* **1954**, *76* (19), 4819-4823. DOI: 10.1021/ja01648a014.

(42) Parsons, R.; Zobel, F. G. R. The interphase between mercury and aqueous sodium dihydrogen phosphate. *Journal of Electroanalytical Chemistry (1959)* **1965**, *9* (5-6), 333-348.

(43) Valette, G. Double layer on silver single-crystal electrodes in contact with electrolytes having anions which present a slight specific adsorption: Part I. The (110) face. *Journal of Electroanalytical Chemistry and Interfacial Electrochemistry* **1981**, *122*, 285-297. DOI: https://doi.org/10.1016/S0022-0728(81)80159-3.

(44) Valette, G. Double layer on silver single crystal electrodes in contact with electrolytes having anions which are slightly specifically adsorbed: Part II. The (100) face. *Journal of Electroanalytical Chemistry and Interfacial Electrochemistry* **1982**, *138* (1), 37-54. DOI: https://doi.org/10.1016/0022-0728(82)87126-X.

(45) Valette, G. Double layer on silver single crystal electrodes in contact with electrolytes having anions which are slightly specifically adsorbed: Part III. The (111) face. *Journal of Electroanalytical Chemistry and Interfacial Electrochemistry* **1989**, *269* (1), 191-203. DOI: https://doi.org/10.1016/0022-0728(89)80112-3.

(46) Hamelin, A.; Stoicoviciu, L. Study of gold low index faces in KPF6 solutions: Part I. Experimental behaviour and determination of the points of zero charge. *Journal of Electroanalytical Chemistry and Interfacial Electrochemistry* **1987**, *234* (1), 93-105. DOI: https://doi.org/10.1016/0022-0728(87)80164-X.

(47) Shin, S.-J.; Kim, D. H.; Bae, G.; Ringe, S.; Choi, H.; Lim, H.-K.; Choi, C. H.; Kim, H. On the importance of the electric double layer structure in aqueous electrocatalysis. *Nature Communications* **2022**, *13* (1), 174. DOI: 10.1038/s41467-021-27909-x.

(48) Pajkossy, T.; Kolb, D. M. On the origin of the double layer capacitance maximum of Pt(111) single crystal electrodes. *Electrochemistry Communications* **2003**, *5* (4), 283-285. DOI: https://doi.org/10.1016/S1388-2481(03)00046-8.

(49) Gebbie, M. A.; Smith, A. M.; Dobbs, H. A.; Warr, G. G.; Banquy, X.; Valtiner, M.; Rutland, M. W.; Israelachvili, J. N.; Perkin, S.; Atkin, R. Long range electrostatic forces in ionic liquids. *Chemical communications* **2017**, *53* (7), 1214-1224.

(50) Gebbie, M. A.; Dobbs, H. A.; Valtiner, M.; Israelachvili, J. N. Long-range electrostatic screening in ionic liquids. *Proceedings of the National Academy of Sciences* **2015**, *112* (24), 7432-7437.
(51) Espinosa-Marzal, R. M.; Arcifa, A.; Rossi, A.; Spencer, N. D. Microslips to "Avalanches" in Confined, Molecular Layers of Ionic Liquids. *The Journal of Physical Chemistry Letters* **2014**, *5* (1), 179-184. DOI: 10.1021/jz402451v.
(52) Gebbie, M. A.; Valtiner, M.; Banquy, X.; Fox, E. T.; Henderson, W. A.; Israelachvili, J. N. Ionic liquids behave as dilute electrolyte solutions. *Proceedings of the National Academy of Sciences* **2013**, *110* (24), 9674-9679.
(53) Smith, A. M.; Lee, A. A.; Perkin, S. The Electrostatic Screening Length in Concentrated Electrolytes Increases with Concentration. *The Journal of Physical Chemistry Letters* **2016**, *7* (12), 2157-2163. DOI: 10.1021/acs.jpclett.6b00867.
(54) Gebbie, M. A.; Smith, A. M.; Dobbs, H. A.; Lee, A. A.; Warr, G. G.; Banquy, X.; Valtiner, M.; Rutland, M. W.; Israelachvili, J. N.; Perkin, S.; et al. Long range electrostatic forces in ionic liquids. *Chemical Communications* **2017**, *53* (7), 1214-1224, 10.1039/C6CC08820A. DOI: 10.1039/C6CC08820A.
(55) Lee, A. A.; Perez-Martinez, C. S.; Smith, A. M.; Perkin, S. Scaling Analysis of the Screening Length in Concentrated Electrolytes. *Physical Review Letters* **2017**, *119* (2), 026002. DOI: 10.1103/PhysRevLett.119.026002.
(56) Pitawela, N. R.; Shaw, S. K. Capacitive Hysteresis Effects in Ionic Liquids: 1-Ethyl-3-methylimidazolium Trifluoromethanesulfonate on Polycrystalline Gold Electrode. *Journal of The Electrochemical Society* **2021**, *168* (4), 046510. DOI: 10.1149/1945-7111/abf4ac.
(57) Uysal, A.; Zhou, H.; Feng, G.; Lee, S. S.; Li, S.; Fenter, P.; Cummings, P. T.; Fulvio, P. F.; Dai, S.; McDonough, J. K.; et al. Structural Origins of Potential Dependent Hysteresis at the Electrified Graphene/Ionic Liquid Interface. *The Journal of Physical Chemistry C* **2014**, *118* (1), 569-574. DOI: 10.1021/jp4111025.
(58) Atkin, R.; Warr, G. G. Structure in Confined Room-Temperature Ionic Liquids. *The Journal of Physical Chemistry C* **2007**, *111* (13), 5162-5168. DOI: 10.1021/jp067420g.
(59) Mezger, M.; Schröder, H.; Reichert, H.; Schramm, S.; Okasinski, J. S.; Schöder, S.; Honkimäki, V.; Deutsch, M.; Ocko, B. M.; Ralston, J.; et al. Molecular layering of fluorinated ionic liquids at a charged sapphire (0001) surface. *Science* **2008**, *322* (5900), 424-428. DOI: 10.1126/science.1164502 From NLM.
(60) Ueno, K.; Kasuya, M.; Watanabe, M.; Mizukami, M.; Kurihara, K. Resonance shear measurement of nanoconfined ionic liquids. *Physical Chemistry Chemical Physics* **2010**, *12* (16), 4066-4071, 10.1039/B923571J. DOI: 10.1039/B923571J.
(61) Hoth, J.; Hausen, F.; Müser, M. H.; Bennewitz, R. Force microscopy of layering and friction in an ionic liquid. *J Phys Condens Matter* **2014**, *26* (28), 284110. DOI: 10.1088/0953-8984/26/28/284110 From NLM.
(62) Zhang, X.; Zhong, Y.-X.; Yan, J.-W.; Su, Y.-Z.; Zhang, M.; Mao, B.-W. Probing double layer structures of Au (111)–BMIPF6 ionic liquid interfaces from potential-dependent AFM force curves. *Chemical Communications* **2012**, *48* (4), 582-584, 10.1039/C1CC15463J. DOI: 10.1039/C1CC15463J.
(63) Maier, F.; Cremer, T.; Kolbeck, C.; Lovelock, K.; Paape, N.; Schulz, P.; Wasserscheid, P.; Steinrück, H.-P. Insights into the surface composition and enrichment effects of ionic liquids and ionic liquid mixtures. *Physical Chemistry Chemical Physics* **2010**, *12* (8), 1905-1915.
(64) Cremer, T.; Stark, M.; Deyko, A.; Steinrück, H. P.; Maier, F. Liquid/solid interface of ultrathin ionic liquid films: [C1C1Im][Tf2N] and [C8C1Im][Tf2N] on Au(111). *Langmuir* **2011**, *27* (7), 3662-3671. DOI: 10.1021/la105007c From NLM.
(65) Han, M.; Kim, H.; Leal, C.; Negrito, M.; Batteas, J. D.; Espinosa-Marzal, R. M. Insight into the Electrical Double Layer of Ionic Liquids Revealed through Its Temporal Evolution. *Advanced Materials Interfaces* **2020**, *7* (24), 2001313. DOI: https://doi.org/10.1002/admi.202001313.
(66) Ma, K.; Jarosova, R.; Swain, G. M.; Blanchard, G. J. Charge-Induced Long-Range Order in a Room-Temperature Ionic Liquid. *Langmuir* **2016**, *32* (37), 9507-9512. DOI: 10.1021/acs.langmuir.6b02639.
(67) Wang, Y.; Jarošová, R.; Swain, G. M.; Blanchard, G. J. Characterizing the Magnitude and Structure-Dependence of Free Charge Density Gradients in Room-Temperature Ionic Liquids. *Langmuir* **2020**, *36* (12), 3038-3045. DOI: 10.1021/acs.langmuir.0c00237.
(68) Bazant, M. Z.; Storey, B. D.; Kornyshev, A. A. Double Layer in Ionic Liquids: Overscreening versus Crowding. *Physical Review Letters* **2011**, *106* (4), 046102. DOI: 10.1103/PhysRevLett.106.046102.
(69) Hammond, O. S.; Bowron, D. T.; Edler, K. J. Liquid structure of the choline chloride-urea deep eutectic solvent (reline) from neutron diffraction and atomistic modelling. *Green Chemistry* **2016**, *18* (9), 2736-2744. DOI: 10.1039/c5gc02914g.
(70) Zhang, Y.; Poe, D.; Heroux, L.; Squire, H.; Doherty, B. W.; Long, Z.; Dadmun, M.; Gurkan, B.; Tuckerman, M. E.; Maginn, E. J. Liquid Structure and Transport Properties of the Deep Eutectic Solvent Ethaline. *The Journal of Physical Chemistry B* **2020**, *124* (25), 5251-5264. DOI: 10.1021/acs.jpcb.0c04058.
(71) Figueiredo, M.; Gomes, C.; Costa, R.; Martins, A.; Pereira, C. M.; Silva, F. Differential capacity of a deep eutectic solvent based on choline chloride and glycerol on solid electrodes. *Electrochimica Acta* **2009**, *54* (9), 2630-2634. DOI: https://doi.org/10.1016/j.electacta.2008.10.074.
(72) Costa, R.; Figueiredo, M.; Pereira, C. M.; Silva, F. Electrochemical double layer at the interfaces of Hg/choline chloride based solvents. *Electrochimica Acta* **2010**, *55* (28), 8916-8920. DOI: https://doi.org/10.1016/j.electacta.2010.07.070.
(73) Vieira, L.; Schennach, R.; Gollas, B. In situ PM-IRRAS of a glassy carbon electrode/deep eutectic solvent interface. *Physical Chemistry Chemical Physics* **2015**, *17* (19), 12870-12880, 10.1039/C5CP00070J. DOI: 10.1039/C5CP00070J.
(74) Chen, Z.; McLean, B.; Ludwig, M.; Stefanovic, R.; Warr, G. G.; Webber, G. B.; Page, A. J.; Atkin, R. Nanostructure of Deep Eutectic Solvents at Graphite Electrode Interfaces as a Function of Potential. *The Journal of Physical Chemistry C* **2016**, *120* (4), 2225-2233. DOI: 10.1021/acs.jpcc.5b10624.
(75) Wu, J.; Zhou, R.; Radjenovic, P. M.; Liu, S.; Wu, D.; Li, J.; Mao, B.; Yan, J. Electrochemical impedance spectroscopy and Raman spectroscopy studies on electrochemical interface between Au(111) electrode and ethaline deep eutectic solvent. *Electrochimica Acta* **2021**, *390*, 138859. DOI: https://doi.org/10.1016/j.electacta.2021.138859.
(76) Kaur, S.; Sharma, S.; Kashyap, H. K. Bulk and interfacial structures of reline deep eutectic solvent: A molecular dynamics study. *The Journal of Chemical Physics* **2017**, *147* (19). DOI: 10.1063/1.4996644 (acccessed 10/30/2023).
(77) Mamme, M. H.; Moors, S. L. C.; Terryn, H.; Deconinck, J.; Ustarroz, J.; De Proft, F. Atomistic Insight into the Electrochemical Double Layer of Choline Chloride-Urea Deep Eutectic Solvents: Clustered Interfacial Structuring. *J Phys Chem Lett* **2018**, *9* (21), 6296-6304. DOI: 10.1021/acs.jpclett.8b01718 From NLM.
(78) Kornyshev, A. A. Double-Layer in Ionic Liquids: Paradigm Change? *The Journal of Physical Chemistry B* **2007**, *111* (20), 5545-5557. DOI: 10.1021/jp067857o.
(79) Kilic, M. S.; Bazant, M. Z.; Ajdari, A. Steric effects in the dynamics of electrolytes at large applied voltages. II. Modified Poisson-Nernst-Planck equations. *Physical Review E* **2007**, *75* (2), 021503. DOI: 10.1103/PhysRevE.75.021503.
(80) Kilic, M. S.; Bazant, M. Z.; Ajdari, A. Steric effects in the dynamics of electrolytes at large applied voltages. I. Double-layer charging. *Physical Review E* **2007**, *75* (2), 021502. DOI: 10.1103/PhysRevE.75.021502.

(81) Oldham, K. B. A Gouy–Chapman–Stern model of the double layer at a (metal)/(ionic liquid) interface. *Journal of Electroanalytical Chemistry* **2008**, *613* (2), 131-138. DOI: https://doi.org/10.1016/j.jelechem.2007.10.017.
(82) Goodwin, Z. A. H.; Feng, G.; Kornyshev, A. A. Mean-Field Theory of Electrical Double Layer In Ionic Liquids with Account of Short-Range Correlations. *Electrochimica Acta* **2017**, *225*, 190-197. DOI: https://doi.org/10.1016/j.electacta.2016.12.092.
(83) Chen, M.; Goodwin, Z. A. H.; Feng, G.; Kornyshev, A. A. On the temperature dependence of the double layer capacitance of ionic liquids. *Journal of Electroanalytical Chemistry* **2018**, *819*, 347-358. DOI: 10.1016/j.jelechem.2017.11.005.
(84) Bi, S.; Banda, H.; Chen, M.; Niu, L.; Chen, M.; Wu, T.; Wang, J.; Wang, R.; Feng, J.; Chen, T.; et al. Molecular understanding of charge storage and charging dynamics in supercapacitors with MOF electrodes and ionic liquid electrolytes. *Nature Materials* **2020**, *19* (5), 552-558. DOI: 10.1038/s41563-019-0598-7.
(85) Goodwin, Z. A. H.; Kornyshev, A. A. Cracking Ion Pairs in the Electrical Double Layer of Ionic Liquids. *Electrochimica Acta* **2022**, *434*, 141163. DOI: https://doi.org/10.1016/j.electacta.2022.141163.
(86) Goodwin, Z. A. H.; McEldrew, M.; Pedro de Souza, J.; Bazant, M. Z.; Kornyshev, A. A. Gelation, clustering, and crowding in the electrical double layer of ionic liquids. *The Journal of Chemical Physics* **2022**, *157* (9). DOI: 10.1063/5.0097055 (acccessed 11/6/2023).
(87) Safran, S. A.; Pincus, P. A. Scaling perspectives of underscreening in concentrated electrolyte solutions. *Soft Matter* **2023**, *19* (41), 7907-7911, 10.1039/D3SM01094E. DOI: 10.1039/D3SM01094E.
(88) Macdonald, J. R.; Barlow, C. A., Jr. Theory of Double-Layer Differential Capacitance in Electrolytes. *The Journal of Chemical Physics* **2004**, *36* (11), 3062-3080. DOI: 10.1063/1.1732426 (acccessed 11/1/2023).
(89) Lauw, Y.; Horne, M. D.; Rodopoulos, T.; Leermakers, F. A. M. Room-Temperature Ionic Liquids: Excluded Volume and Ion Polarizability Effects in the Electrical Double-Layer Structure and Capacitance. *Physical Review Letters* **2009**, *103* (11), 117801. DOI: 10.1103/PhysRevLett.103.117801.
(90) Merlet, C.; Limmer, D. T.; Salanne, M.; van Roij, R.; Madden, P. A.; Chandler, D.; Rotenberg, B. The Electric Double Layer Has a Life of Its Own. *The Journal of Physical Chemistry C* **2014**, *118* (32), 18291-18298. DOI: 10.1021/jp503224w.
(91) Kornyshev, A. A.; Qiao, R. Three-Dimensional Double Layers. *The Journal of Physical Chemistry C* **2014**, *118* (32), 18285-18290. DOI: 10.1021/jp5047062.
(92) Wang, S.; Zhang, J.; Gharbi, O.; Vivier, V.; Gao, M.; Orazem, M. E. Electrochemical impedance spectroscopy. *Nature Reviews Methods Primers* **2021**, *1* (1), 41.
(93) Córdoba-Torres, P.; Mesquita, T. J.; Nogueira, R. P. Relationship between the Origin of Constant-Phase Element Behavior in Electrochemical Impedance Spectroscopy and Electrode Surface Structure. *The Journal of Physical Chemistry C* **2015**, *119* (8), 4136-4147. DOI: 10.1021/jp512063f.
(94) Reichert, P.; Kjær, K. S.; Brandt van Driel, T.; Mars, J.; Ochsmann, J. W.; Pontoni, D.; Deutsch, M.; Nielsen, M. M.; Mezger, M. Molecular scale structure and dynamics at an ionic liquid/electrode interface. *Faraday Discussions* **2018**, *206* (0), 141-157, 10.1039/C7FD00171A. DOI: 10.1039/C7FD00171A.
(95) Drüschler, M.; Huber, B.; Roling, B. On Capacitive Processes at the Interface between 1-Ethyl-3-methylimidazolium tris(pentafluoroethyl)trifluorophosphate and Au(111). *The Journal of Physical Chemistry C* **2011**, *115* (14), 6802-6808. DOI: 10.1021/jp200395j.
(96) Lockett, V.; Horne, M.; Sedev, R.; Rodopoulos, T.; Ralston, J. Differential capacitance of the double layer at the electrode/ionic liquids interface. *Physical Chemistry Chemical Physics* **2010**, *12* (39), 12499-12512, 10.1039/C0CP00170H. DOI: 10.1039/C0CP00170H.
(97) Jitvisate, M.; Seddon, J. R. T. Direct Measurement of the Differential Capacitance of Solvent-Free and Dilute Ionic Liquids. *The Journal of Physical Chemistry Letters* **2018**, *9* (1), 126-131. DOI: 10.1021/acs.jpclett.7b02946.
(98) Gore, T. R.; Bond, T.; Zhang, W.; Scott, R. W.; Burgess, I. J. Hysteresis in the measurement of double-layer capacitance at the gold–ionic liquid interface. *Electrochemistry communications* **2010**, *12* (10), 1340-1343.
(99) Zhou, W.; Xu, Y.; Ouchi, Y. Hysteresis effects in the in situ SFG and differential capacitance measurements on metal electrode/ionic liquids interface. *ECS Transactions* **2013**, *50* (11), 339.
(100) Drüschler, M.; Huber, B.; Passerini, S.; Roling, B. Hysteresis effects in the potential-dependent double layer capacitance of room temperature ionic liquids at a polycrystalline platinum interface. *The Journal of Physical Chemistry C* **2010**, *114* (8), 3614-3617.
(101) Uysal, A.; Zhou, H.; Feng, G.; Lee, S. S.; Li, S.; Fenter, P.; Cummings, P. T.; Fulvio, P. F.; Dai, S.; McDonough, J. K. Structural origins of potential dependent hysteresis at the electrified graphene/ionic liquid interface. *The Journal of Physical Chemistry C* **2014**, *118* (1), 569-574.
(102) Lucio, A. J.; Shaw, S. K. Effects and controls of capacitive hysteresis in ionic liquid electrochemical measurements. *Analyst* **2018**, *143* (20), 4887-4900, 10.1039/C8AN01085D. DOI: 10.1039/C8AN01085D.
(103) Lucio, A. J.; Shaw, S. K.; Zhang, J.; Bond, A. M. Large-Amplitude Fourier-Transformed AC Voltammetric Study of the Capacitive Electrochemical Behavior of the 1-Butyl-3-methylimidazolium Tetrafluoroborate–Polycrystalline Gold Electrode Interface. *The Journal of Physical Chemistry C* **2017**, *121* (22), 12136-12147. DOI: 10.1021/acs.jpcc.7b00287.
(104) Lucio, A. J.; Shaw, S. K.; Zhang, J.; Bond, A. M. Double-Layer Capacitance at Ionic Liquid–Boron-Doped Diamond Electrode Interfaces Studied by Fourier Transformed Alternating Current Voltammetry. *The Journal of Physical Chemistry C* **2018**, *122* (22), 11777-11788. DOI: 10.1021/acs.jpcc.8b00272.
(105) Klein, J. M.; Panichi, E.; Gurkan, B. Potential dependent capacitance of [EMIM][TFSI], [N1114][TFSI] and [PYR13][TFSI] ionic liquids on glassy carbon. *Physical Chemistry Chemical Physics* **2019**, *21* (7), 3712-3720, 10.1039/C8CP04631J. DOI: 10.1039/C8CP04631J.
(106) Jeffrey, M. K. Electroanalytical Investigation of the Electrode–Electrolyte Interface of Quaternary Ammonium Ionic Liquids: Impact of Alkyl Chain Length and Ether Functionality. *Journal of physical chemistry* **2019**, *v. 124* (no. 10), pp. 5613-5623-2019 v.5124 no.5610. DOI: 10.1021/acs.jpcc.9b08016 From National Agricultural Library PubAg.
(107) Li, H.; Endres, F.; Atkin, R. Effect of alkyl chain length and anion species on the interfacial nanostructure of ionic liquids at the Au(111)–ionic liquid interface as a function of potential. *Physical Chemistry Chemical Physics* **2013**, *15* (35), 14624-14633, 10.1039/C3CP52421C. DOI: 10.1039/C3CP52421C.
(108) Dean, W.; Penley, D.; Lee, Y.-Y.; Ghahremani, R.; Dongare, S.; Gurkan, B. Anion Effects on the Interfacial Structure and Bulk Physical Properties in Choline-Based Hydrogen-Bonded Electrolytes. *The Journal of Physical Chemistry C* **2022**, *126* (34), 14598-14610. DOI: 10.1021/acs.jpcc.2c01901.
(109) Silvester, D. S.; Jamil, R.; Doblinger, S.; Zhang, Y.; Atkin, R.; Li, H. Electrical Double Layer Structure in Ionic Liquids and Its Importance for Supercapacitor, Battery, Sensing, and Lubrication Applications. *The Journal of Physical Chemistry C* **2021**, *125* (25), 13707-13720. DOI: 10.1021/acs.jpcc.1c03253.
(110) Kaaliveetil, S.; Lee, Y.-Y.; Li, Z.; Cheng, Y.-H.; Menon, N. H.; Dongare, S.; Gurkan, B.; Basuray, S. Ionic Liquid-Packed Microfluidic Device with Non-Planar Microelectrode as a Miniaturized Electrochemical Gas Sensor. *Journal of The*

Electrochemical Society **2023**, *170* (8), 087508. DOI: 10.1149/1945-7111/aced6e.
(111) Luo, T.; Liu, K.; Fu, J.; Chen, S.; Li, H.; Pan, H.; Liu, M. Electric Double Layer Structure in Electrocatalytic Carbon Dioxide Reduction. *Advanced Energy and Sustainability Research* **2023**, *4* (3), 2200148. DOI: https://doi.org/10.1002/aesr.202200148 (acccessed 2023/10/24).
(112) Simon, P.; Gogotsi, Y. Materials for electrochemical capacitors. *Nature Materials* **2008**, *7* (11), 845-854. DOI: 10.1038/nmat2297.
(113) Frackowiak, E.; Béguin, F. Carbon materials for the electrochemical storage of energy in capacitors. *Carbon* **2001**, *39* (6), 937-950. DOI: https://doi.org/10.1016/S0008-6223(00)00183-4.
(114) Xu, N.; Klein, J. M.; Huang, P.; Alwusaydi, H. A.; Mann, E. K.; Gurkan, B. E. Improved accessibility of porous carbon electrodes with surfactant ionic liquids for supercapacitors. *Journal of Applied Electrochemistry* **2019**, *49* (2), 151-162. DOI: 10.1007/s10800-018-1266-3.
(115) Massicot, S.; Sasaki, T.; Lexow, M.; Shin, S.; Maier, F.; Kuwabata, S.; Steinrück, H.-P. Adsorption, Wetting, Growth, and Thermal Stability of the Protic Ionic Liquid Diethylmethylammonium Trifluoromethanesulfonate on Ag(111) and Au(111). *Langmuir* **2021**, *37* (39), 11552-11560. DOI: 10.1021/acs.langmuir.1c01823.
(116) Costa, R.; Brandão, A. T. S. C.; Pereira, C. M.; Silva, A. F. Electrified interfaces of deep eutectic solvents. *Electrochimica Acta* **2023**, *461*, 142653. DOI: https://doi.org/10.1016/j.electacta.2023.142653.
(117) Jiang, X.; Wu, X.; Xie, Y.; Wang, Z.; Huang, J.; Qu, Y.; Mu, D.; Zhang, X.; Yang, W.; Zhang, H. Additive Engineering Enables Ionic-Liquid Electrolyte-Based Supercapacitors To Deliver Simultaneously High Energy and Power Density. *ACS Sustainable Chemistry & Engineering* **2023**, *11* (14), 5685-5695. DOI: 10.1021/acssuschemeng.3c00213.
(118) Atilhan, M.; Costa, L. T.; Aparicio, S. Elucidating the Properties of Graphene–Deep Eutectic Solvents Interface. *Langmuir* **2017**, *33* (21), 5154-5165. DOI: 10.1021/acs.langmuir.7b00767.
(119) Largeot, C.; Portet, C.; Chmiola, J.; Taberna, P.-L.; Gogotsi, Y.; Simon, P. Relation between the Ion Size and Pore Size for an Electric Double-Layer Capacitor. *Journal of the American Chemical Society* **2008**, *130* (9), 2730-2731. DOI: 10.1021/ja7106178.
(120) Chmiola, J.; Yushin, G.; Gogotsi, Y.; Portet, C.; Simon, P.; Taberna, P. L. Anomalous Increase in Carbon Capacitance at Pore Sizes Less Than 1 Nanometer. *Science* **2006**, *313* (5794), 1760-1763. DOI: 10.1126/science.1132195 (acccessed 2023/10/24).
(121) Dyatkin, B.; Osti, N. C.; Zhang, Y.; Wang, H.-W.; Mamontov, E.; Heller, W. T.; Zhang, P.; Rother, G.; Cummings, P. T.; Wesolowski, D. J.; et al. Ionic liquid structure, dynamics, and electrosorption in carbon electrodes with bimodal pores and heterogeneous surfaces. *Carbon* **2018**, *129*, 104-118. DOI: https://doi.org/10.1016/j.carbon.2017.12.001.
(122) Lian, C.; Liu, K.; Van Aken, K. L.; Gogotsi, Y.; Wesolowski, D. J.; Liu, H. L.; Jiang, D. E.; Wu, J. Z. Enhancing the Capacitive Performance of Electric Double-Layer Capacitors with Ionic Liquid Mixtures. *ACS Energy Letters* **2016**, *1* (1), 21-26. DOI: 10.1021/acsenergylett.6b00010.
(123) Puttaswamy, R.; Mondal, C.; Mondal, D.; Ghosh, D. An account on the deep eutectic solvents-based electrolytes for rechargeable batteries and supercapacitors. *Sustainable Materials and Technologies* **2022**, *33*, e00477. DOI: https://doi.org/10.1016/j.susmat.2022.e00477.
(124) Perkin, S. Ionic liquids in confined geometries. *Physical Chemistry Chemical Physics* **2012**, *14* (15), 5052-5062, 10.1039/C2CP23814D. DOI: 10.1039/C2CP23814D.
(125) Kondrat, S.; Feng, G.; Bresme, F.; Urbakh, M.; Kornyshev, A. A. Theory and Simulations of Ionic Liquids in Nanoconfinement. *Chemical Reviews* **2023**, *123* (10), 6668-6715. DOI: 10.1021/acs.chemrev.2c00728.
(126) Bernasconi, R.; Lucotti, A.; Nobili, L.; Magagnin, L. Ruthenium Electrodeposition from Deep Eutectic Solvents. *Journal of The Electrochemical Society* **2018**, *165* (13), D620. DOI: 10.1149/2.0541813jes.
(127) Manolova, M.; Böck, R.; Scharf, I.; Mehner, T.; Lampke, T. Electrodeposition of Pd alloys from choline chloride/urea deep eutectic solvents. *Journal of Alloys and Compounds* **2021**, *855*, 157462. DOI: https://doi.org/10.1016/j.jallcom.2020.157462.
(128) Abbott, A. P.; Ballantyne, A.; Harris, R. C.; Juma, J. A.; Ryder, K. S.; Forrest, G. A Comparative Study of Nickel Electrodeposition Using Deep Eutectic Solvents and Aqueous Solutions. *Electrochimica Acta* **2015**, *176*, 718-726. DOI: https://doi.org/10.1016/j.electacta.2015.07.051.
(129) Natter, H.; Bukowski, M.; Hempelmann, R.; Abedin, S. Z. E.; Moustafa, E. M.; Endres, F. Electrochemical Deposition of Nanostructured Metals and Alloys from Ionic Liquids. *Zeitschrift für Physikalische Chemie* **2006**, *220* (10), 1275-1291. DOI: doi:10.1524/zpch.2006.220.10.1275 (acccessed 2023-12-31).
(130) Abbott, A. P.; Frisch, G.; Ryder, K. S. Electroplating using ionic liquids. *Annual Review of Materials Research* **2013**, *43*, 335-358.
(131) Böttcher, R.; Mai, S.; Borisenko, N.; Ispas, A.; Bund, A.; Endres, F. A Raman Study on the Speciation of Different Metal Ions in an AlCl3–Based Ionic Liquid. *Journal of The Electrochemical Society* **2023**, *170* (7), 072503.
(132) Li, Z.; Wang, J.; Xie, H.; Yu, K.; Song, Q.; Ning, Z. Electrodeposition of Al foil for the collector of lithium-ion batteries by electrorefining in [Emim] Cl-AlCl3 ionic liquid with O2− ion at room temperature: Electrochemical dissolution behavior of Al anode. *Electrochimica Acta* **2023**, 142743.
(133) Lenka, R.; Reddy, R. G. Rare Earth and Critical Base Metals Electrodeposition Using Urea-Choline Chloride Ionic Liquids. In *TMS Annual Meeting & Exhibition*, 2023; Springer: pp 151-159.
(134) Litaiem, Y.; Dridi, D.; Slimi, B.; Chtourou, R. Electrodeposition of Cadmium Selenide Based Photoanodes from TOMAC/Formamide Ionic Liquid System for Photoelectrochemical Water Splitting. *International Journal of Nanoscience* **2023**, *22* (02), 2350013.
(135) Huddleston, J. G.; Visser, A. E.; Reichert, W. M.; Willauer, H. D.; Broker, G. A.; Rogers, R. D. Characterization and comparison of hydrophilic and hydrophobic room temperature ionic liquids incorporating the imidazolium cation. *Green Chemistry* **2001**, *3* (4), 156-164, 10.1039/B103275P. DOI: 10.1039/B103275P.
(136) Shaheen, N. A.; Ijjada, M.; Vukmirovic, M. B.; Akolkar, R. Mechanism of Electrochemical Oxidation of Nitroxide Radicals in Ethaline Deep Eutectic Solvent. *Journal of The Electrochemical Society* **2020**, *167* (14), 143505.
(137) Shaheen, N. A.; Dean, W.; Penley, D.; Kersten, B.; Rintamaki, J.; Vukmirovic, M. B.; Gurkan, B. E.; Akolkar, R. Electro–Oxidation of Nitroxide Radicals: Adsorption–Mediated Charge Transfer Probed Using SERS and Potentiometry. *Journal of The Electrochemical Society* **2022**, *169* (5), 053511. DOI: 10.1149/1945-7111/ac7082.
(138) Chen, B.; Mitchell, S.; Sinclair, N.; Wainright, J.; Pentzer, E.; Gurkan, B. Feasibility of TEMPO-functionalized imidazolium, ammonium and pyridinium salts as redox-active carriers in ethaline deep eutectic solvent for energy storage. *Molecular Systems Design & Engineering* **2020**, *5* (6), 1147-1157, 10.1039/D0ME00038H. DOI: 10.1039/D0ME00038H.
(139) Klein, J. M.; Squire, H.; Dean, W.; Gurkan, B. E. From Salt in Solution to Solely Ions: Solvation of Methyl Viologen in Deep Eutectic Solvents and Ionic Liquids. *The Journal of Physical Chemistry B* **2020**, *124* (29), 6348-6357. DOI: 10.1021/acs.jpcb.0c03296.
(140) Ghahremani, R.; Dean, W.; Sinclair, N.; Shen, X.; Starvaggi, N.; Alfurayj, I.; Burda, C.; Pentzer, E.; Wainright, J.; Savinell, R.; et al. Redox-Active Eutectic Electrolyte with Viologen and

Ferrocene Derivatives for Flow Batteries. *ACS Applied Materials & Interfaces* **2023**, *15* (1), 1148-1156. DOI: 10.1021/acsami.2c18546.
(141) Xiao, L.; Wildgoose, G. G.; Compton, R. G. Investigating the voltammetric reduction of methylviologen at gold and carbon based electrode materials. Evidence for a surface bound adsorption mechanism leading to electrode 'protection' using multi-walled carbon nanotubes. *New Journal of Chemistry* **2008**, *32* (9), 1628-1633, 10.1039/B804842H. DOI: 10.1039/B804842H.
(142) Hahn, C.; Jaramillo, T. F. Using Microenvironments to Control Reactivity in CO2 Electrocatalysis. *Joule* **2020**, *4* (2), 292-294. DOI: https://doi.org/10.1016/j.joule.2020.01.017.
(143) Klemm, A.; Vicchio, S. P.; Bhattacharjee, S.; Cagli, E.; Park, Y.; Zeeshan, M.; Dikki, R.; Liu, H.; Kidder, M. K.; Getman, R. B.; et al. Impact of Hydrogen Bonds on CO2 Binding in Eutectic Solvents: An Experimental and Computational Study toward Sorbent Design for CO2 Capture. *ACS Sustainable Chemistry & Engineering* **2023**, *11* (9), 3740-3749. DOI: 10.1021/acssuschemeng.2c06767.
(144) Dikki, R.; Cagli, E.; Penley, D.; Karayilan, M.; Gurkan, B. Formation of choline salts and dipolar ions for CO2 reactive eutectic solvents. *Chemical Communications* **2023**, *59* (80), 12027-12030, 10.1039/D3CC03272H. DOI: 10.1039/D3CC03272H.
(145) Zeeshan, M.; Kidder, M. K.; Pentzer, E.; Getman, R. B.; Gurkan, B. Direct air capture of CO2: from insights into the current and emerging approaches to future opportunities. *Frontiers in Sustainability* **2023**, *4*, Perspective. DOI: 10.3389/frsus.2023.1167713.
(146) Moura de Salles Pupo, M.; Kortlever, R. Electrolyte Effects on the Electrochemical Reduction of CO2. *ChemPhysChem* **2019**, *20* (22), 2926-2935. DOI: https://doi.org/10.1002/cphc.201900680.
(147) Rosen, B. A.; Salehi-Khojin, A.; Thorson, M. R.; Zhu, W.; Whipple, D. T.; Kenis, P. J.; Masel, R. I. Ionic liquid–mediated selective conversion of CO2 to CO at low overpotentials. *Science* **2011**, *334* (6056), 643-644.
(148) Rosen, B. A.; Haan, J. L.; Mukherjee, P.; Braunschweig, B.; Zhu, W.; Salehi-Khojin, A.; Dlott, D. D.; Masel, R. I. In Situ Spectroscopic Examination of a Low Overpotential Pathway for Carbon Dioxide Conversion to Carbon Monoxide. *The Journal of Physical Chemistry C* **2012**, *116* (29), 15307-15312. DOI: 10.1021/jp210542v.
(149) Baldelli, S. Probing electric fields at the ionic liquid-electrode interface using sum frequency generation spectroscopy and electrochemistry. *J Phys Chem B* **2005**, *109* (27), 13049-13051. DOI: 10.1021/jp052913r From NLM.
(150) Atkin, R.; Borisenko, N.; Drüschler, M.; El Abedin, S. Z.; Endres, F.; Hayes, R.; Huber, B.; Roling, B. An in situSTM/AFM and impedance spectroscopy study of the extremely pure 1-butyl-1-methylpyrrolidinium tris(pentafluoroethyl)trifluorophosphate/Au(111) interface: potential dependent solvation layers and the herringbone reconstruction. *Physical Chemistry Chemical Physics* **2011**, *13* (15), 6849-6857, 10.1039/C0CP02846K. DOI: 10.1039/C0CP02846K.
(151) Kirchner, K.; Kirchner, T.; Ivaništšev, V.; Fedorov, M. V. Electrical double layer in ionic liquids: Structural transitions from multilayer to monolayer structure at the interface. *Electrochimica Acta* **2013**, *110*, 762-771. DOI: https://doi.org/10.1016/j.electacta.2013.05.049.
(152) Kamalakannan, S.; Prakash, M.; Chambaud, G.; Hochlaf, M. Adsorption of Hydrophobic and Hydrophilic Ionic Liquids at the Au(111) Surface. *ACS Omega* **2018**, *3* (12), 18039-18051. DOI: 10.1021/acsomega.8b02163.
(153) García Rey, N.; Dlott, D. D. Structural Transition in an Ionic Liquid Controls CO2 Electrochemical Reduction. *The Journal of Physical Chemistry C* **2015**, *119* (36), 20892-20899. DOI: 10.1021/acs.jpcc.5b03397.
(154) Dongare, S.; Coskun, O. K.; Cagli, E.; Lee, K. Y. C.; Rao, G.; Britt, R. D.; Berben, L. A.; Gurkan, B. A Bifunctional Ionic Liquid for Capture and Electrochemical Conversion of CO2 to CO over Silver. *ACS Catalysis* **2023**, *13* (12), 7812-7821. DOI: 10.1021/acscatal.3c01538.
(155) Coskun, O. K.; Dongare, S.; Doherty, B.; Klemm, A.; Tuckerman, M.; Gurkan, B. Tailoring Electrochemical CO2 Reduction on Copper by Reactive Ionic Liquid and Native Hydrogen Bond Donors. *Angewandte Chemie International Edition* n/a (n/a), e202312163. DOI: https://doi.org/10.1002/anie.202312163.

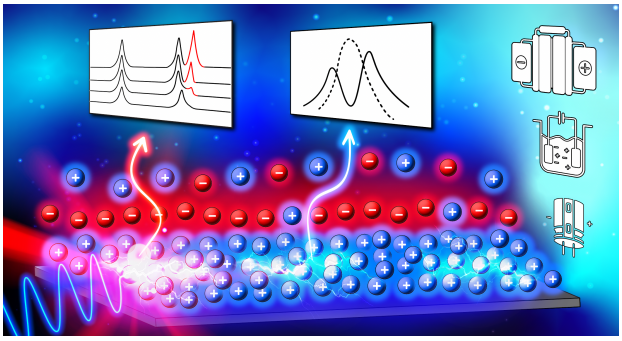

Biographies

Oguz Kagan Coskun is a Ph.D. student at Case Western Reserve University under the supervision of Burcu Gurkan. He completed his B.S. in Metallurgical and Materials Engineering, and M.Sc. in Materials Science and Engineering at Istanbul Technical University focusing on molten salt electrolysis. His research interests involve electrode-electrolyte interfaces, electrocatalyst materials, ionic liquid electrolytes, and analytical and computational electrochemistry.

Miguel is a Ph.D. student at Case Western Reserve University under the supervision of Burcu Gurkan. Miguel is currently a member of the US Department of Energy Early Career Network through BEES2 EFRC. He has a B.S. in Biological and Pharmaceutical Chemistry and an M.S. in Chemical Science and Technology from the Autonomous University of Zacatecas, Mexico. His research aims to advance sustainable energy storage solutions by developing deep eutectic solvents and protic ionic liquids as electrolytes for redox flow batteries. Miguel combines density functional theory calculations with advanced spectroscopic and electrochemical characterization methods.

Saudagar Dongare is a Postdoctoral Researcher at Case Western Reserve University under the supervision of Burcu Gurkan. Dr. Dongare is currently a member of the US Department of Energy Early Career Network through 4C EFRC. He received his Ph.D. in Chemical Engineering in 2021 from Thapar Institute of Engineering and Technology, India. His research interests involve environmental electrocatalysis, developing electrode materials and electrolytes for electrochemical CO_2 reduction, and studying the electrode-electrolyte interfaces with in-situ spectroscopy.

William Dean is currently a Postdoctoral Researcher at Argonne National Laboratory in USA. He successfully earned his Ph.D. in Chemical Engineering from Case Western Reserve University in 2023. Dr Dean served as the chair of Student Research Organization of BEES EFRC. the William's dedicated research centers around electrolyte exploration, with a particular emphasis on the electrode-electrolyte interface, and the characterization for electrochemical storage applications. Additionally, his expertise extends to the chemical and electrochemical separation of actinide species.

Burcu (Eksioglu) Gurkan joined Chemical and Biomolecular Engineering Department at Case Western Reserve University as an Assistant Professor in 2016, rising through the ranks to Professor in 2023. Her research focuses on the physical properties and reactivity in deep eutectic solvents and ionic liquids for applications in separations, energy storage and conversion. She completed her B.S. degree in Chemical Engineering from the Middle East Technical University in Turkey, Ph.D. degree from the University of Notre Dame, and Post-doctoral trainings at the Massachusetts Institute of Technology and The University of Akron. She is the Deputy Director of BEES2 (Breakthrough Electrolytes for Energy Storage Systems) – a Department of Energy Frontier Research Center (EFRC) and a Key Researcher in 4C (Center for Closing the Carbon Cycle) EFRC where she leads the effort in developing structured electrolytes for electrochemical processes for flow batteries and CO_2 conversion, respectively.